The Pivotal Role of s-, p-, and f-Block Metals in Water Electrolysis: Status Quo and Perspectives

Ziliang Chen, Hongyuan Yang, Zhenhui Kang,* Matthias Driess,* and Prashanth W. Menezes*

Transition metals, in particular noble metals, are the most common species in metal-mediated water electrolysis because they serve as highly active catalytic sites. In many cases, the presence of nontransition metals, that is, s-, p-, and f-block metals with high natural abundance in the earth-crust in the catalytic material is indispensable to boost efficiency and durability in water electrolysis. This is why alkali metals, alkaline-earth metals, rare-earth metals, lean metals, and metalloids receive growing interest in this research area. In spite of the pivotal role of these nontransition metals in tuning efficiency of water electrolysis, there is far more room for developments toward a knowledge-based catalyst design. In this review, five classes of nontransition metals species which are successfully utilized in water electrolysis, with special emphasis on electronic structure–catalytic activity relationships and phase stability, are discussed. Moreover, specific fundamental aspects on electrocatalysts for water electrolysis as well as a perspective on this research field are also addressed in this account. It is anticipated that this review can trigger a broader interest in using s-, p-, and f-block metals species toward the discovery of advanced polymetal-containing electrocatalysts for practical water splitting.

1. Introduction

The ever-increasing consumption of fossil fuels combined with worldwide environmental concerns is forcing the rapid development of sustainable energy sources.[1] To overcome this severe circumstance, tremendous effort has been devoted to the exploration of electrochemical conversion and storage devices, such as water splitting, electrochemical reduction of nitrogen and carbon dioxide, fuel cell, rechargeable batteries, and electrosynthesis technologies.[2] Among them, water splitting is of particular interest because of its readily coupling with renewable wind and solar power to produce hydrogen fuel with high purity.[3,4] However, the thermodynamically uphill and sluggish kinetics of both hydrogen evolution reaction (HER) and oxygen evolution reaction (OER) of water splitting inevitably degrades the overall energy efficiency.[5] To address this issue, highly efficient electrocatalysts are indispensable to lower the energy barrier and to accelerate the OER and HER reaction. Currently, numerous transition metal-based compounds have been demonstrated as promising electrocatalysts toward water splitting.[6]

Transition metals that are located in the d-block region of the periodic table contain non-noble and noble metals. Among them, noble metals refer to eight elements including Au, Ag, and the platinum group metals (Rh, Ru, Pd, Os, Ir, Pt), which are located in the fifth and sixth periods of the periodic table. In terms of water splitting, the highest active electrocatalysts toward HER and OER are Pt- and Ru/Ir-based materials, respectively, which appreciably deliver high current densities at low overpotentials.[7] Unfortunately, two drawbacks have severely blocked the widespread application of these noble metal-based catalysts. On the one hand, noble metals are suffering from limited natural abundance, leading to a relatively high market price.[8] On the other hand, noble metal atoms on the surface undergo agglomeration and dissolution (leaching) during electrocatalysis, resulting in poor endurance.[9] Consequently, a great deal of attention has been paid to simultaneously reduce the amount of noble metal and increasing the catalyst durability. It has been well documented that physically hybridizing nanosized noble metal-based compounds with carbon matrices[10–14] and chemically binding of single noble metal

Z. Chen, Z. Kang
Institute of Functional Nano and Soft Materials (FUNSOM)
Jiangsu Key Laboratory for Carbon-Based Functional Materials and Devices
Soochow University
Suzhou 215123, P. R. China
E-mail: zhkang@suda.edu.cn
Z. Chen, H. Yang, M. Driess, P. W. Menezes
Department of Chemistry
Metalorganics and Inorganic Materials
Technische Universität Berlin
Straße des 17 Juni 135, Sekr. C2, 10623 Berlin, Germany
E-mail: matthias.driess@tu-berlin.de;
prashanth.menezes@mailbox.tu-berlin.de
P. W. Menezes
Material Chemistry Group for Thin Film Catalysis – CatLab
Helmholtz-Zentrum Berlin für Materialien und Energie
Albert-Einstein-Str. 15, 12489 Berlin, Germany

atoms with special support[15–18] are two powerful tricks to alleviate the above issues. By carbon hybridization, the aggregation of nanosized noble metal-based compounds can be effectively inhibited.[19–23] Meanwhile, this approach can also be greatly conducive to the dispersion of active sites of noble metals and the decrease of the usage of noble metal species. With respect to the carbon hybridization strategy, through downsizing the noble metal entity from bulk to nanoparticle and cluster to a single atom, nearly 100% of metal utilization rate can be gradually achieved because it can expose all active metal atom sites during the electrochemical reaction, thus essentially deceasing the usage of noble metal.[24,25] In addition, quantum size effects of the single atom can generate discrete energy level distributions, e.g., highest occupied molecular orbital–lowest unoccupied molecular orbital gaps, allowing foreign atom doping-induced asymmetrical spin and charge density.[26,27] Furthermore, the robust interaction of the single metal atom with certain supports can prominently facilitate the charge and ion transfer during the electrochemical reaction.[28] These merits enable single atom catalysis theoretically to acquire extraordinarily high catalytic selectivity, activity, and stability.

Besides the two aforementioned strategies, the doping of noble metal-based systems with non-noble transition metals (e.g., Fe, Co, Ni, Cu, Mn, W, Mo, herein abbreviate them as NNTM) is also a viable strategy.[29,30] NNTM with partially electron-filled d-valence orbitals can easily donate or gain electrons upon coupling with noble metals. Taking Pt–NNTM alloys as an example, the charge coupling between Pt and NNTM as well as the strain effect caused by the solid solution of NNTM within the Pt lattice can effectively tune the d-band center, thus optimizing the free adsorption energy of H intermediate.[31,32] Moreover, if the structurally ordered Pt–NNTM alloy is generated, the inherent NNTM–Pt bond hosted in the intermetallic remarkably enhances the work stability against electrolyte corrosion during catalysis.[33,34] The partial doping of noble metals with NNTM can also decrease the catalyst expense owing to the much lower cost of NNTM as compared to noble ones. Inspired by the above premises, the majority of research began to shift the focus from noble metal (oxides), NNTM-doped noble metal (oxides) to NNTM compounds (e.g., NNTM alloys, oxides, phosphides, chalcogenides, nitrides, carbon-coupled NNTMs, and single NNTM atoms).[35–38] Moreover, the optimization efforts adapted for solely NNTM-based electrocatalysts have also been derived from the noble metal-based ones to perform efficient catalysis. Beyond the noble metal counterparts, it is worthy to mention that the investigations on electrocatalysts constructed by chemically binding NNTM with nonmetals (e.g., P, S, Se, Te) for water splitting have been exceptional and achieved huge progress over the past decades.[39,40] Nevertheless, with respect to the NNTM or their alloys, the wide application was generally hindered by two aspects.[36,41] One is their unsatisfactory adsorption free energy toward the HER and OER intermediates, resulting in the moderate intrinsic catalytic capability, and the other one is their high tendency to undergo corrosion in basic and acidic solution, leading to undesirable durability. Within the NNTM-based oxides/chalcogenides/phosphides, most of them suffer from low intrinsic conductivity, and they are usually transformed to the corresponding metal (oxy)hydroxides, which also hold the low conductivity, leading to the poor charge

transfer ability.[36,42] Similarly, the practical application of the single NNTM atoms is still hindered by the complicated fabrication procedure and the ideal coordination to realize the excellent bifunctional activity toward water splitting.[43] Therefore, the design of NNTM-based systems as electrocatalysts and their functional role during catalysis still needs to be further enriched from the point of developing practical electrocatalysts.

Recently, some preliminary works corroborated the unique function of nontransition metal species belonging to the s-, p-, and f-block elements of the periodic table in improving catalytic activity.[44–46] In practical terms, these s-, p-, and f-block metals (herein abbreviate them as SPFM for the following description) are distinguished by five types, i.e., alkali metals, alkaline-earth metals, lean metals (in the basic metal region), metalloids, and rare-earth metals (mainly refers to the lanthanide metals) (**Figure 1**). These metal species were mostly reported as the core component subunit, which was incorporated into NNTM-based compounds to tune the catalytic activity. The series of research in this direction may open new directions for the design of advanced catalytic classes, namely, the metal-based electrocatalysts that can be extended from noble metal-based, NNTM-mediated noble metal-based, NNTM-based to SPFM-mediated NNTM-based, or even the SPFM-based system,[47–71] however, the discussion related to this topic has never been documented in the literature although successive reviews focused on the design, modification, and application of d-block transition metal-based electrocatalysts for water splitting have been consistently reported.[72–75]

Motivated by the above concern, the objective of this comprehensive contribution is to present an opportune overview of the encouraging work on the roles of SPFM during water splitting, by which more insightful research in this burgeoning field is expected to grow. We begin this review with a brief introduction of the two half-reaction pathways, followed by a discussion of activity guidance and the connotation of precatalysts. Then, going beyond the scope of transition metal-based electrocatalysts, the recent progress of five types of nontransition metal species for water splitting is elucidated in detail, aiming at establishing their influence on the electronic structure, phase stability, as well as catalytic behavior of the whole (pre)catalyst system, thus obtaining the dependence of activity on composition and structure. Additionally, this review also highlights the formidable challenges with respect to the future development of these nontransition metal species for electrolysis.

2. Basic Understanding of (Pre)catalysts toward Water Electrolysis

2.1. Catalytic Mechanism of HER and OER

Water splitting contains two half-reactions, HER and OER, and they present different reaction pathways in acidic versus alkaline media (**Table 1**).[76,77] The HER is composed of Volmer/Heyrovsky or Volmer/Tafel steps as shown in **Figure 2**A. According to the reaction pathways, four intermediate steps including water adsorption, water dissociation, OH-adsorption, and hydrogen binding are involved in the alkaline HER process. Water adsorption is the first step of hydrogen evolution
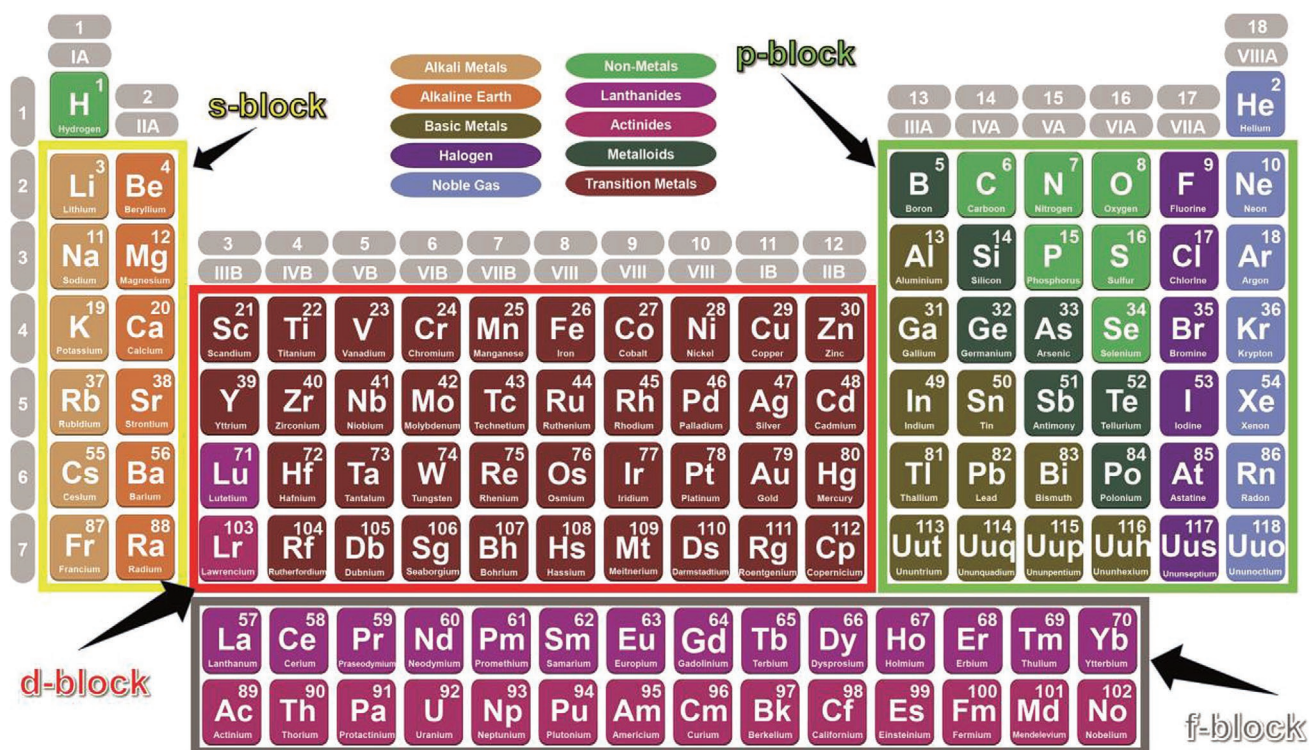
Figure 1. The periodic table of s-, p-, d-, and f-block elements.

in alkaline media, which exhibits a much higher energy barrier than the H_3O^+ adsorption in acidic media. For some electrocatalysts (e.g., Pt), the activity of HER in the alkaline media is theoretically two orders of magnitude lower than that in acidic media. It is believed that the rational design of electrocatalysts with a strong capability to dissociate water and bind protons will notably improve the alkaline HER performance.[76,77]

As depicted in Figure 2B, the OER process in the alkaline media usually involves the following four steps.[78,79] First, on the premise of surface metal sites (M) as a catalytically active site, the intermediate M–OH is formed via one-electron oxidation of hydroxide anion. Thereafter, the M–OH turns into M–O after a proton coupling and electron transfer, and then the M–O gets converted into M–OOH after a hydroxide anion coupled with one-electron oxidation and finally initiating another proton-coupled electron transfer process to generate O_2. Slightly different from the OER process in the alkaline media, the adsorption of water molecule onto M is the first step in the acidic media (Figure 2C) and then dissociation of a proton to form M–OH, followed by the release of the second proton to yield M–O is the subsequent step. Next, another water molecule undergoes a nucleophilic attack on M–O, resulting in the formation of M–OOH. Finally, the O_2 was desorbed from the active sites accompanied by the fourth proton coupling. In fact, another pathway combining two M–O species to directly form O_2 has also been reported in alkaline media.[76] However, because of the compositional instability in acidic media, the surface of these NNTM-based compounds during OER is likely to be changed and deactivated. In recent years, with more special effort devoted to the investigation of the OER mechanism,

the lattice oxygen participation mechanism (LOM) has also been proposed, which is different from the above-mentioned adsorbate evolution-dominated mechanism (AEM). Taking the alkaline LOM mechanism as an example (Figure 2D),[80] in the first step, the hydroxyl is adsorbed on the oxygen vacancy (V_O)-coordinated metal site (M–OH/–V_O). Next, the V_O site near the M site adsorbs an additional hydroxyl (M–OH/–OH), namely, a hydroxyl filling reaction. Following that, a dehydrogenation process occurs and generates M–OH/–O. However, the hydroxyl is not easy to directly undergo further dehydrogenation, and thus a transition state (M–OHO, not shown in the figure) is formed. Because this transition state is unstable, it subsequently converts into M–OO/–V_O. Finally, upon releasing the oxygen and filling hydroxyl, the initial state M–OH/–V_O is recovered again. The acidic LOM mechanism is similar to the alkaline one, and the major difference is the generation of H^+ and the absence of OH^- in each step (Table 1). In the LOM process, the lattice oxygen of catalysts directly participates in oxygen evolution and formation of oxygen molecules, leading to more efficient catalysis.[78,80]

2.2. Design Strategies Enabling the High Catalytic Activity

The overpotential (η), Faradaic efficiency, and durability are the critical indices to assess the HER and OER activity, which have been elaborately introduced in previous literature.[78–82] The catalytic activity is a sum of the intrinsic part and extrinsic part. The intrinsic activity can be reflected from the Tafel slope (b), turnover frequency (TOF), charge transfer resistance

Table 1. Reaction pathways for the electrocatalyst in acidic and alkaline media.

| Reaction type	Media	Overall reaction	Intermediate reaction steps
HER	Acidic AEM	$2H^+ + 2e^- \leftrightarrow H_2$	$M + H^+ + e^- \rightarrow M–H$ $M–H + H^+ + e^- \rightarrow M + H_2$ (Heyrovsky step) $M–H + M–H \rightarrow 2M + H_2$ (Tafel step)
	Alkaline AEM	$2H_2O + 2e^- \leftrightarrow H_2 + 2OH^-$	$M + H_2O + e^- \rightarrow M–H + OH^-$ $M–H + H_2O + e^- \rightarrow M + OH^- + H_2$ (Heyrovsky step) $M–H + M–H \rightarrow 2M + H_2$ (Tafel step)
OER	Acidic AEM	$2H_2O \rightarrow O_2 + 4H^+ + 4e^-$	$M + H_2O \rightarrow M–OH + H^+ + e^-$ $M–OH \rightarrow M–O + H^+ + e^-$ $M–O + H_2O \rightarrow M–OOH + H^+ + e^-$ $M–OOH \rightarrow M + O_2 + H^+ + e^-$
	Alkaline AEM	$4OH^- \rightarrow O_2 + 2H_2O + 4e^-$	$M + OH^- \rightarrow M–OH + e^-$ $M–OH + OH^- \rightarrow M–O + H_2O + e^-$ $M–O + OH^- \rightarrow M–OOH + e^-$ $M–OOH + OH^- \rightarrow M + O_2 + H_2O + e^-$
	Acidic LOM	$2H_2O \rightarrow O_2 + 4H^+ + 4e^-$	$(M–OH + V_O) + H_2O \rightarrow M–OH/–OH + H^+ + e^-$ $M–OH/–OH \rightarrow M–OH + H^+ + e^-$ $M–OH + H_2O \rightarrow (M–OO + V_O) + H^+ + e^-$ $(M–OO + V_O) + H_2O \rightarrow (M–OH + V_O) + O_2 + H^+ + e^-$
	Alkaline LOM	$4OH^- \rightarrow O_2 + 2H_2O + 4e^-$	$(M–OH + V_O) + OH^- \rightarrow M–OH/–OH + e^-$ $M–OH/–OH + OH^- \rightarrow M–OH/–O + H_2O + e^-$ $M–OH + OH^- \rightarrow (M–OO + V_O) + H_2O + e^-$ $(M–OO + V_O) + OH^- \rightarrow (M–OH + V_O) + O_2 + e^-$

(R_{ct}), and Gibbs free adsorption energy (ΔG_{ad}) toward H-/O-containing intermediates. Tafel slope is regarded as an important descriptor to check the dominant reaction mechanism and reaction kinetics within a certain potential window. The TOF represents the ability of an electrocatalyst to produce the desired product per catalytic site as a function of time and is an indication of the intrinsic catalytic activity of each catalytic site.[83] The R_{ct} is correlated with the interface charge transfer ability of the electrode. A lower R_{ct} value indicates a faster reaction rate. The ΔG_{ad} is popularly employed as a vital descriptor to estimate the intrinsic activity. To be specific, as the competitive adsorption and desorption of H-/O-containing intermediates occur during the HER and OER process, only the best balance between absorption and desorption energy results in a good catalytic performance.

The extrinsic activity can be reflected from the electrochemical active surface area (ECSA) and surface structure, which is associated with the number of active sites, the utilization of active sites as well as the mass diffusion ability. A larger ECSA value usually suggests the more potential catalytic active sites which can participate in the catalytic reaction. The surface structure of the catalyst usually refers to the porosity and surface area, where the porosity including pore volume and pore size distribution is closely related to the mass transport, while the surface area has a large influence on the accessibility of the active sites. As such, in order to render the electrocatalyst with low overpotential, high Faradaic efficiency, and long-term durability toward HER and OER, an electrocatalyst should possess both impressive intrinsic and extrinsic activity. Therefore, understanding how to design the advanced electrocatalysts to achieve satisfactory HER and OER activity is of great significance. To date, several general design strategies such as the component modulation (e.g., the hybridization of metal with

anion), external field stimulation (e.g., magnetic, light), electronic regulation (e.g., d-band tuning), phase engineering (e.g., polymorphic transformation), electrode optimization (e.g., self-supporting electrode), and morphology tuning (e.g., porous hollow architecture) have been proposed to realize this goal (Figure 2E).[78–87] Among them, the former four tend to improve the intrinsic activity while the latter two are prone to enhance extrinsic activity. In many instances, these strategies are synergistically adopted to coenhance the catalytic activity.

2.3. Connotation of Precatalyst

Although the catalytic pathways and the general strategies to improve the catalytic performance have been proposed, a deep understanding of some unique electrocatalysts still needs to be further acquired because of their diversity and complexity. Especially, recent investigations have revealed that a variety of NNTM-based electrocatalysts undergo a phase reconstruction during the HER and OER tests, and then these reconstructed phases were served as the real active sites for catalysis.[85–94] These electrocatalysts are now commonly viewed as the precatalyst, which holds huge potential as cheap and efficient HER and OER electrocatalysts because of their attractive qualities including the in situ converted porous nanodomains, optimized electronic structure, and highly intrinsic catalytic active sites. Currently, there are three possible models in terms of the phase reconstruction (**Figure 3**A):[95,96] i) near-surface reconstruction, ii) partial reconstruction (core–shell), and iii) complete reconstruction. Obviously, the phase conversion tendency is gradually strengthened from model (i) to model (iii). In general, a deeper reconstruction can be more beneficial for better catalytic activity. Furthermore, the tendency or the degree of the phase
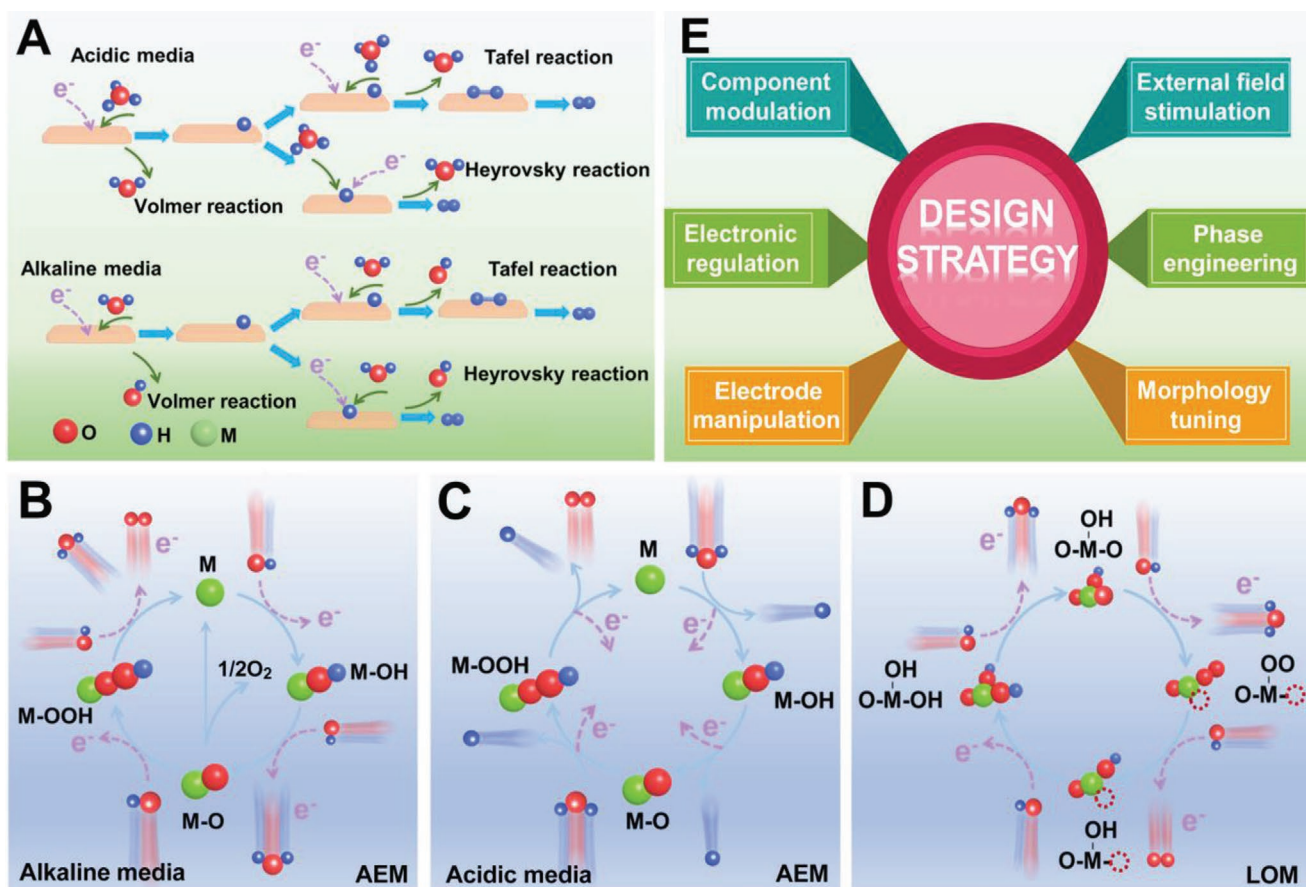
Figure 2. A) HER mechanism in acidic and alkaline media. Adsorbate evolution mechanism (AEM) in B) alkaline media and C) acidic media for OER. D) The lattice oxygen participation mechanism (LOM) for alkaline OER. E) Optimization strategies for efficient HER and OER electrocatalysts. The red, green, and blue spheres in (A)–(D) represent the O, M, and H atoms, while the dotted red circle in (D) denotes the oxygen vacancy.

reconstruction against the catalysis is highly dependent on the operation condition, crystal structure, (micro)morphology, and chemical composition (Figure 3B).

The operation condition including applied potential, electrolyte concentration, working temperature, pH value, and reaction type plays a critical role in phase reconstruction.[97] It is well-known that the required potential to drive OER (usually higher than 1.5 V vs RHE) on the catalyst is generally more positive than the equilibrium potential. When the applied potential surpasses the redox potential of the NNTM species in electrocatalysts, the valence state of these elements changed accordingly and turned to the formation of oxygen-containing intermediates, which readily cause the phase instability. Once such a redox process is (partial) irreversible, a cycle test will give rise to the phase reconstruction on the surface of the catalyst. Compared to the OER, the applied potential for HER is more negative than the equilibrium potential to produce hydrogen. In this case, a reduction reaction usually occurs which leads to the generation of a metallic state of the catalysts. The phase reconstruction behavior in different electrolyte media is also very different. In both the alkaline and acidic media, leaching or corrosion accompanied by the chemical reduction can usually be observed for electrocatalysts in the HER process, leading to the surface-rich metal layer. However, most of these NNTM-based

electrocatalysts show poor stability during the OER process in the acidic media because of the serious leaching, whereas the phase reconstruction can be well observed in the alkaline media.[78] Besides the applied potential, reaction type, and pH value, recent reports also indicated that a deeper reconstruction could be triggered via implementing a higher working temperature or higher concentrated electrolyte within a rational range, by which the reaction kinetics was accelerated.[97]

In terms of the phase structure, both the amorphous structure and defect feature are supposed to be beneficial for phase reconstruction.[40,98,99] This is because in these two cases, there are many unsaturated coordinated NNTM atoms, where electrolyte as well as the hydrogen/oxygen-containing groups, are much easier to be accessible to these atoms, thus expediting the atom leaching and the phase evolution during the electrochemically driven reaction. Moreover, the crystal lattice such as the polymorphism also influences the degree of phase reconstruction.[] For instance, under the identical test condition, the orthorhombic-type $CoSe_2$ with defects showed a deeper degree of the reconstruction as compared to that of the cubic-type $CoSe_2$ phase during both OER and HER.[101] However, a general descriptor still needs to be further explored for guiding the design of crystal lattice, which is favorable to phase reconstruction. On the other hand, there is no doubt that the morphology

**ADVANCED
SCIENCE NEWS**

www.advancedsciencenews.com

**ADVANCED
MATERIALS**

www.advmat.de
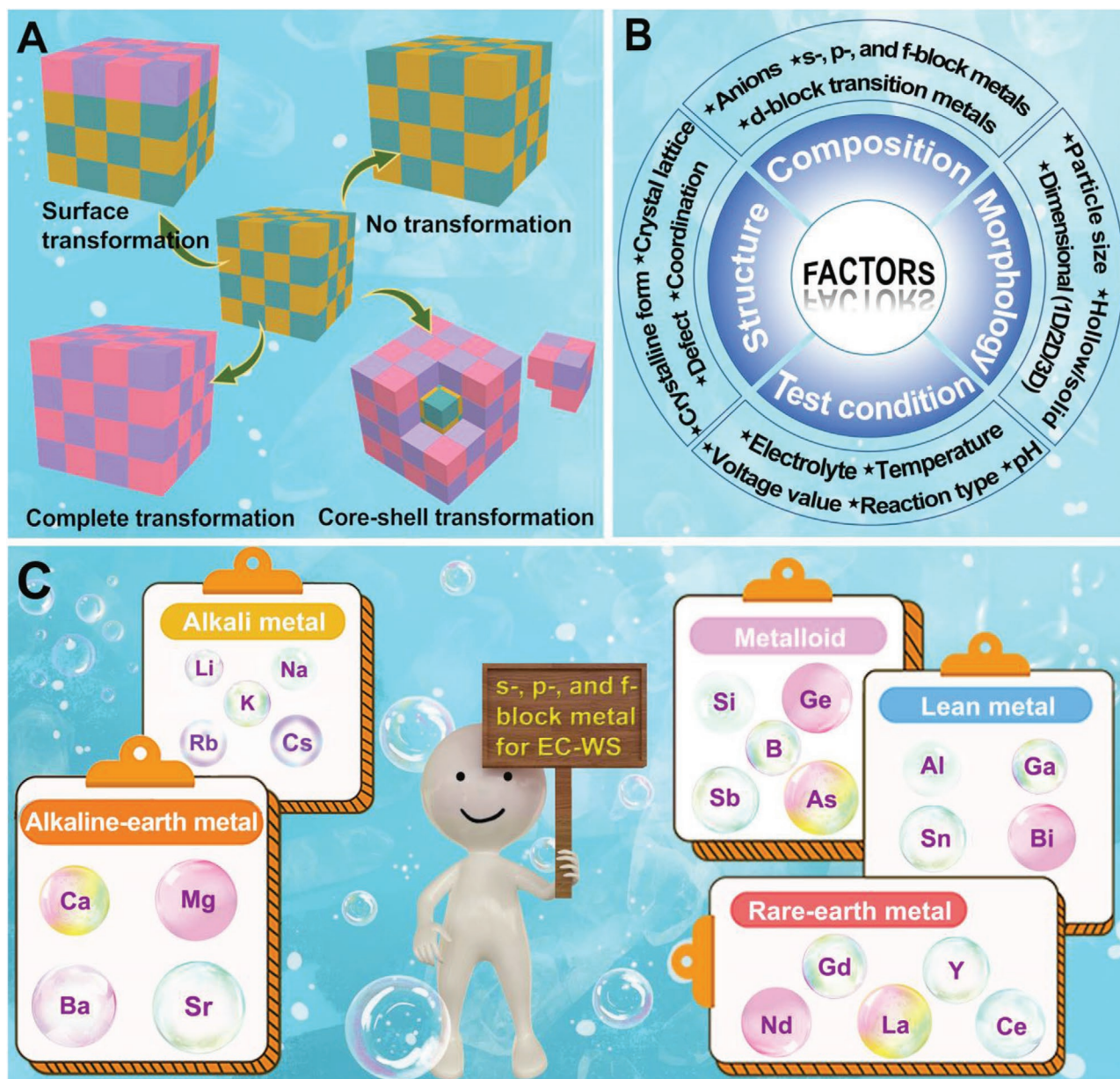
Figure 3. A) Phase evolution pathways against the HER and/or OER process. B) General factors influencing the phase evolution. C) Schematic illustration for five classes of nontransition metal for the usual construction of electrocatalysts toward electrochemical water splitting (EC-WS).

of the precatalyst also has an effect on phase reconstruction. Especially the particle size of the precatalyst, as pointed out by previous literature,[97–99] where the phase reconstruction mostly initiates at the surface of NNTMO particles. When the reconstructed dense layer reaches around 10 nm, it tends to prevent the penetration of H- or OH-ligands into the inner bulk for further reduction or oxidation. Thus, the nanosized active particle can achieve a high reconstruction degree.[97] On the basis of the nanostructuring, the construction of nanorods, nanosheets, or hollow nanopolyhedra can be better for the phase reconstruction because of the sufficient exposure of NNTM sites as well as the intensive affinity between the active site and protons or electrons.

The phase composition that can be etched and/or embraces the redox metal is a prerequisite for the phase reconstruction of the catalyst in the catalytic process.[101,102] At present, NNTM with anions are widely investigated as the core components of precatalyst, especially combining them as NNTM sulfides, tellurides, phosphides, nitrides, etc.[102] In these compounds, the anions promote the instability of catalysts in the reaction process and accelerate the phase reconstruction centered on NNTMs. Interestingly, when we summarized the role of five classes of nontransition metals in catalysis (Figure 3C), we found that most of them have been playing a critical role in phase reconstruction, which has been presented in the subsequent sections.

**ADVANCED
SCIENCE NEWS**

www.advancedsciencenews.com

**ADVANCED
MATERIALS**

www.advmat.de

3. Merits of s-, p-, and f-Block Metals in Water Electrolysis

Unlike transition metals, SPFMs have rarely been reported as direct active sites due to their limited redox chemistry and the number of oxidation states. Nevertheless, they can be served as a subunit mediator to guide the catalytic activity of NNTM-based electrocatalysts. As illustrated in **Figure 4**, the incorporation of SPFM species into NNTM-based compounds can play the following nine main roles in improving the catalytic activity. Specifically, i) the leaching of SPFM species or the coupling of SPFM-based phase with NNTM-based ones will destabilize the precatalyst and accelerate the phase transformation to the active NNTM-based (oxy)(hydro)oxides during catalysis, contributing to generate the porously active nanodomains with more active sites;[68] ii) the presence of these SPFM species within NNTM-based phase will alter the charge distribution around NNTM atoms, and thus probably optimize the free adsorption energy of active site toward oxygen- and hydrogen-containing intermediates during OER and HER;[70] iii) these SPFM-based phase can function as the confinement matrix to trap the single NNTM atom or cluster, which will enable a nearly 100% utilization of active sites;[103] iv) if the SPFM-based phase is inert during the catalysis, its strong coupling with NNTM-based phase could inhibit the agglomeration of the newly formed NNTM-based (oxy)(hydro)oxides, which are reconstructed from NNTM-based precatalysts, and thereby a sufficient exposure of active sites;[71] v) the insertion of SPFM into the layer lattice of NNTM-based catalysts or that of the transformed NNTM-based (hydro)oxides is beneficial to the mass transfer and diffusion, accelerating the reaction kinetics especially at the large current density;[66] vi) the SPFM can combine with the NNTM to form the intermetallics, which possesses the metallic nature and high conductivity, being in favor of the charge transfer;[92] vii) some SPFM atoms are inactive during catalysis, but their presence is beneficial to the dissociation of water molecular on the surface of catalyst and shift the proton or hydroxyl radical to the surrounding active sites, resulting in the decrease of the reaction energy barrier;[104] viii) the introduction of these SPFM into NNTM-based compounds will change the morphology of the composite during synthesis, e.g., the formation of 1D, 2D, and 3D nanoarchitecture, which is helpful to the exposure of active sites, intimate contact between active site and electrolyte as well as the enhancement of structural stability;[105] and ix) certain SPFM atoms hosted in the NNTM-based precatalysts hold the intrinsic photothermal effect.[106] In this case, upon the injection of light into the catalyst during water splitting, a local thermal effect could be triggered, by which the reaction kinetics will be greatly expedited. It should be noted that the improvement mechanism of catalytic activity is highly dependent on the SPFM species, which has been comprehensively elucidated in the successive sections.

3.1. Insights Into the Improvement of Activity by Alkali Metals

Alkali metals bear lower toxicity and costs compared to those of NNTMs. Meanwhile, except Rb and Cs, they can be easily found on earth's surface, crust, and in the ocean, which makes them quite sustainable and appealing. In addition, alkali metals are highly reactive chemical species, presenting a fairly simple electronic configuration and offering a chance to function as electron donors when chemically bonded with other components.[107] Bearing that in mind, there has recently been a booming interest in exploring their tuning toward NNTM-based electrocatalysts for efficient water electrolysis. Currently, the alkali metals are basically introduced into three material systems including NNTM-based oxides, hydroxides, and chalcogenides to modify their OER and/or HER activity.[108–132] The aims of introducing alkali metals mainly contain the following three aspects.[111–128] First, the appropriate introduction of alkali metal ions into NNTM-based compound can enhance the oxidation state of NNTM species, by which the electrophilicity of NNTM toward the adsorbed O is effectively increased, and thus accordingly promoting the reaction of one OH-anion with one adsorbed O atom on NNTM to form the adsorbed OOH-intermediate. Second, the NNTM–O(S) bond becomes more covalent upon the incorporation of appropriate alkali metal ions, by which a hole state near the Fermi level is created and the hybridization of O(S) 2p–NNTM 3d is enhanced, enabling the catalyst more electrophilic and even activating lattice oxygen as active sites. Finally, although enormous NNTM-based oxides or sulfides are semiconductors, the appropriate introduction of alkali metal ions will make the catalyst metallic, and hence the efficient charge transport during catalysis is achieved. In terms of the NNTM-based oxide, in an early study, Cui and co-workers synthesized $Li_{0.5}CoO_2$ by an electrochemical lithium tuning method, which could deliver a much better OER activity than that of benchmark Ir-based electrocatalyst.[111] Following this observation, Yan and co-workers proposed a chemical sodium extraction method to derive the $NaNi_yFe_{1-y}O_2$ into the $Na_{1-x}Ni_yFe_{1-y}O_2$, which could also present a remarkable OER catalytic activity.[112] Interestingly, Yan and co-workers claimed that based on the $Na_{0.7}CoO_2$ derived from $NaCoO_2$ by the electrochemical sodium tuning method, further insertion of other metal ions such as Ag and Cu could induce an apparent lattice strain, which was helpful for optimizing the free adsorption energy of the Co active site toward OH^-, leading to the superior OER activity than that of Ru-based electrocatalysts.[113] To unveil the composition–electronic structure–activity correlation for OER electrocatalysts, by a synergistic combination of synchrotron-based photoemission spectroscopy, X-ray absorption spectroscopy (XAS), and density functional theory (DFT), Zhang and co-workers found that with the increase of the Li-doping amount into $Li_xNi_{1-x}O$ from 0 to 0.5, the oxidation state of Ni was increased (**Figure 5**A).[114] Moreover, a new hole state at 1.1 eV above the Fermi level emerged and the hybridization degree of O 2p-Ni 3d was intensified (Figure 5B), which optimized the adsorption energy of OH-intermediates (Figure 5C). More broadly, the alkali metal ions-doping induced the improvement of OER activity that can be applied to a variety of NNTM oxides including spined oxide,[115] perovskite,[116] and rock salt.[117]

Unlike NNTM-based oxides to some extent, the incorporation of alkali-metal ions into the NNTM-based oxyhydroxide can additionally enlarge the layer spacing by creating the cation-oxygen coordination (Figure 5D), facilitating the mass transfer during OER catalysis.[120,121] Since the alkali-metal ion
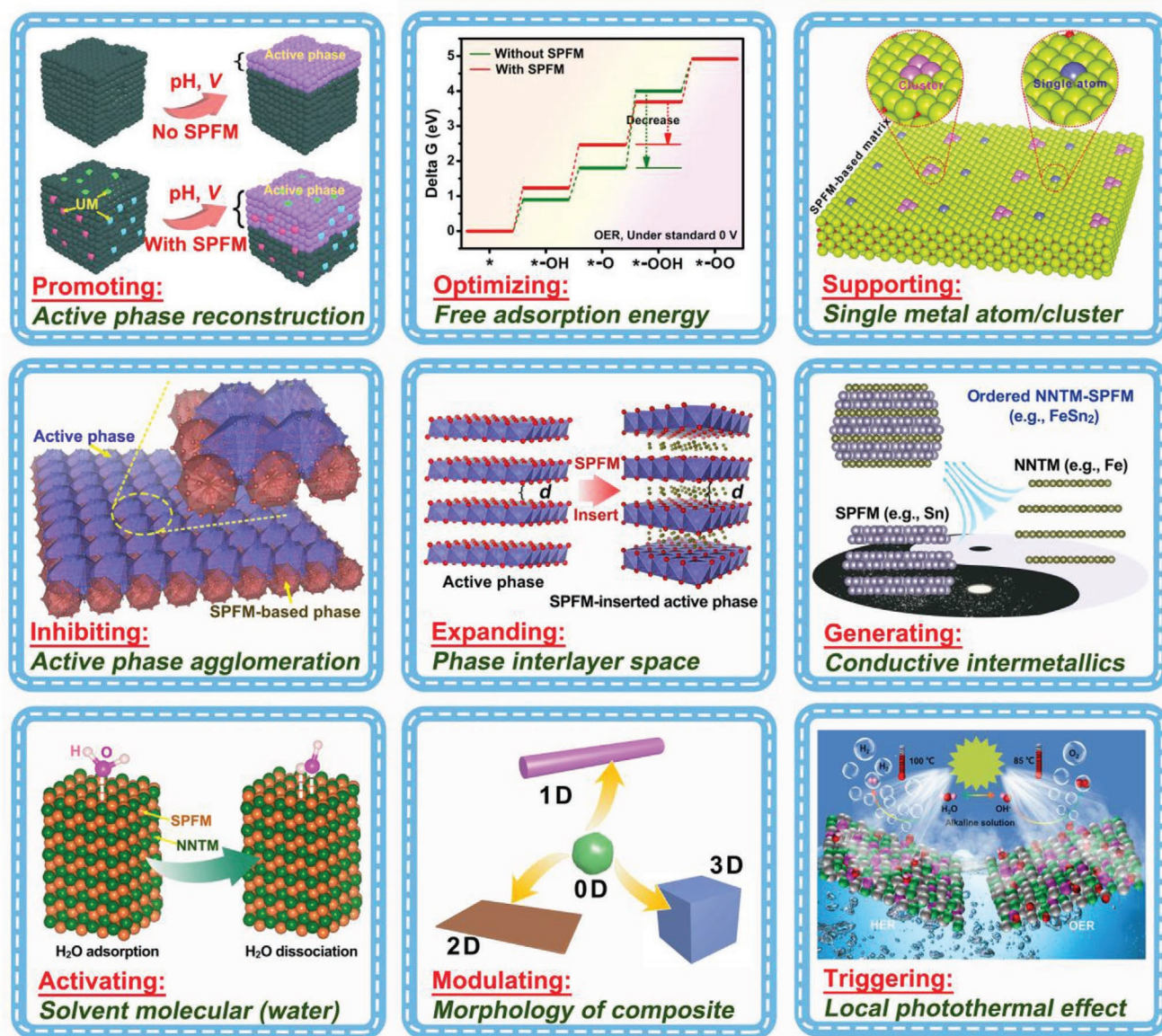
Figure 4. The pivotal roles of s-, p-, and f-block metal species in tuning the catalytic activity of electrocatalysts.

size enlarges in the order of $Li^+ < Na^+ < K^+ < Rb^+ < Cs^+$, several physical and chemical properties regularly varied, such as the gradual decrease of electronegativity and Lewis acidity, increase of the proton affinity, molar conductivity as well as the basicity of the corresponding alkali hydroxide counterparts.[122–124] Koper and co-workers examined the effect of the alkali cation (Li^+, Na^+, K^+, and Cs^+) on the OER activity of Ni(Fe)OOH catalysts.[126] With the incorporation of alkali cations into Ni(Fe)OOH, an improved OER activity followed the order of $Li^+ < K^+ \leq Na^+ < Cs^+$. Two mechanisms responsible for the impact of alkali cations on the OER activity have been put forward: i) small alkali metal cations hold a higher tendency to generate strong noncovalent interactions with the chemisorbed species to form solvation shells that block the active sites, resulting in the sluggish reorientation and kinetics;[127] ii) as compared to the alkali metal ions with a small radius, those with large radius

readily contribute to the creation of peroxo-like "active oxygen" species (O^- or O^{2-}) in NiOOH, thus lowering the energy barrier during OER process.[129,130] However, the above hypothesis could not be deployed to explain several inconsistencies in the activity trends, e.g., the activity of Ni(Fe)OOH was lower in CsOH compared to that in both NaOH and KOH.[126,133] Motivated by this, Diaz-Morales and co-workers recently proposed a new mechanism, that is, the Lewis acidity of the alkali cations changed the electrolyte pH, which then affected the OER activity.[134] This can account for the puzzling discrepancy that the OER activity of Cs^+-tuned Ni(Fe)OOH was lower compared to Na^+- and K^+-tuned ones. To be specific, by an in situ XAS test of Ni(Fe)OOH in different alkali metal-ions electrolytes during OER catalysis (Figure 5E–G), it was found that the alkali cation radius-induced activity differences were relatively small, and the pH for electrolyte was the critical influence factor. Although
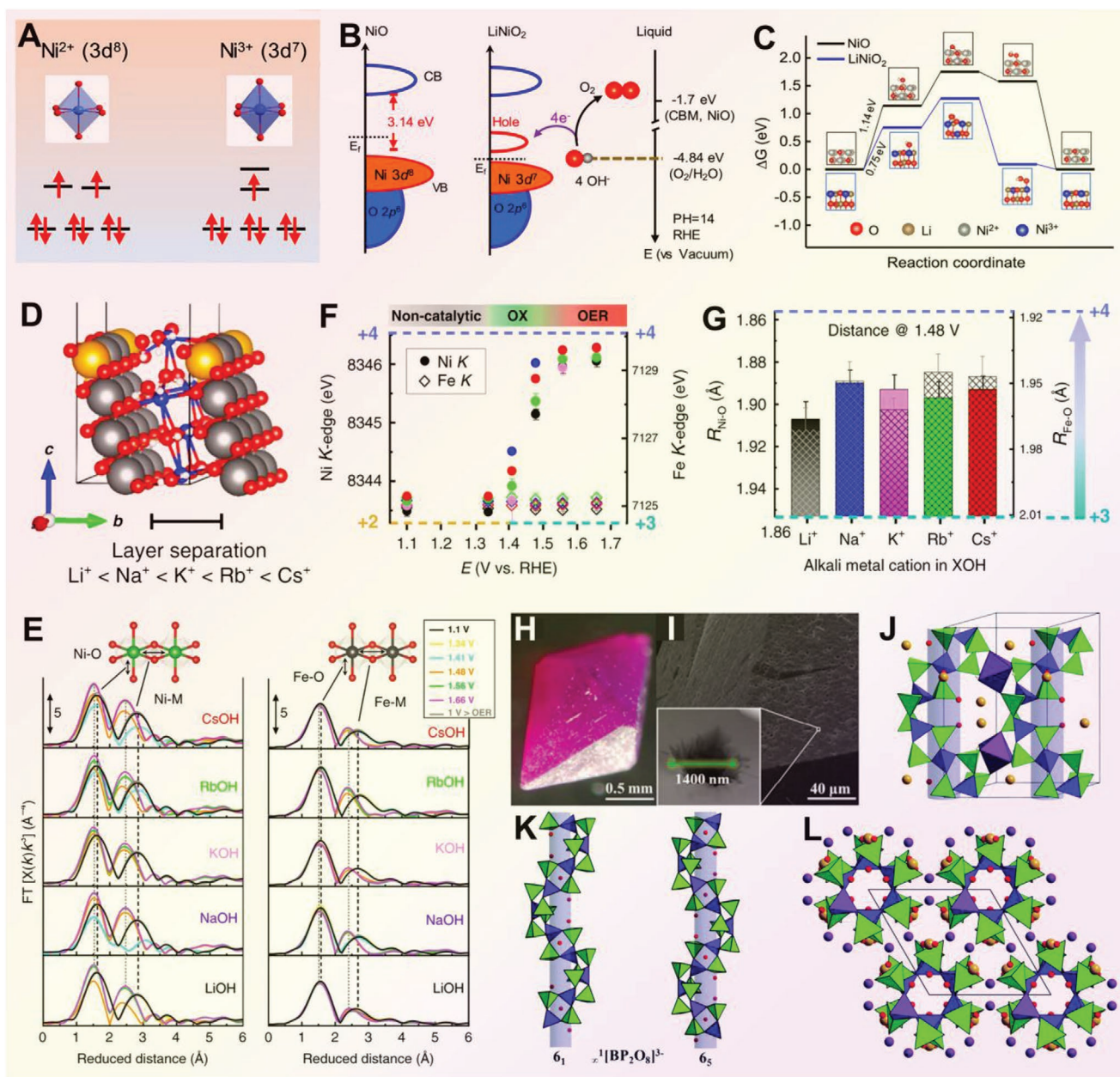
Figure 5. A) The corresponding Ni^{2+} and Ni^{3+} d-electron states in octahedral crystal field splitting. B) Schematic diagram for electronic structures of NiO and $LiNiO_2$ (left) and energy diagram at the oxide-liquid interface. C) Calculated free energy profiles of NiO and $LiNiO_2$ for OER under 1.23 V. Reproduced with permission.[114] Copyright 2019, American Chemical Society. D) Surface model of γ-Ni(Fe)OOH(100) with intercalating alkali metal cations. E) The k^3-weighted Fourier-transformed EXAFS at the Ni K-edges and Fe K-edges. F) Ni and Fe K-edge positions versus the applied potential. The colored areas on top indicate the different regions (noncatalytic, oxidative "OX", and "OER" catalytic). G) Trend-plots of the Ni–O and Fe–O coordination distances at 1.48 V versus the alkali metal cation (X) in the XOH electrolyte. Reproduced with permission.[134] Copyright 2020, Nature Publishing Group. H,I) Microscopic and J–L) schematic structure of alkali metal helical borophosphates, green, violet, and fuchsia polyhedra represents PO_4, BO_4, and $CoO_4(OH_2)_2$, respectively. Alkali metals are shown in yellow spheres. Reproduced with permission.[139] Copyright 2019, The Royal Society of Chemistry.

the concentrations of different alkali cations were the same, both the pH of the electrolyte and the OER activity of electrocatalysts were different. Furthermore, the dependence of current density on the pH value at 1.56 V was approached to a linear relationship with an increased slope of 30 mA cm^{-2} pH^{-1}. Correspondingly, the dependence of potential on the pH value at 5 mA cm^{-2} was also approached to a linear relationship with

a decreased slope of 80 mV pH^{-1}. When the pH for each electrolyte was adjusted to a near-identical value, the OER activity indeed align more closely, and easily showed a different activity trend upon adjusting another pH value. In view of this, the lower OER activity of Cs^+-tuned Ni(Fe)OOH could be attributed to the deviation of pH value as compared to those of Na^+- and K^+-tuned Ni(Fe)OOH, which caused by the synergistic factors

ADVANCED
SCIENCE NEWS
www.advancedsciencenews.com

ADVANCED
MATERIALS
www.advmat.de

of the different hygroscopic feature of alkali metal ions-salt and different Lewis acidity of atoms around Fe atoms.

NNTM-based oxides and oxyhydroxides are considered as the potential OER electrocatalysts, while NNTM-based chalcogenides usually are good candidates for HER reactions.[135] In this context, $NaFeS_2$,[136] as well as, a series of Li/Na/K-tuned Co_9S_8[137] and WSe_2[138] were synthesized and investigated as HER electrocatalysts. The incorporation of alkali metals greatly enhanced the conductivity and optimized the free adsorption energy toward H-intermediate, making these electrocatalysts deliver an outstanding HER activity comparable to those of Pt-based electrocatalysts. In addition to the above-mentioned compounds, it should be pointed out that exploring the novel class of alkali metal-containing compounds as HER and OER electrocatalysts is of great interest. Recently, Menezes et al. reported that porous crystalline alkali-metal cobalt borophosphates (LiCoBPO and NaCoBPO) with chiral DNA-like helical structure could exhibit remarkable HER and OER activity (Figure 5H–L).[139] Unprecedently, depending on the applied electrode potential, these catalysts can be reversibly switched between catalysis of the HER and OER at low overpotentials, along with impressive long-term stability of more than two months. Further structural characterization by quasi in situ XAS revealed that the structural reconstruction occurred during both the OER and HER process, where the former generated the active cobalt (oxy)hydroxide phase while the latter produced the active Co/CoO_x phase, accompanied by the leaching of alkali-metal species. Similar observations were also made with alkali metal manganese borophosphates (LiMnBPO and NaMnBPO) where during OER the initial structures transformed into porous and defect-rich amorphous layered birnessite MnO_x with exceptional durability over five months.[140] Further study by Song and co-workers revealed that the leaching of alkali metals from the helical unit during catalysis left lattice vacancies, leading to the favorable adsorption of intermediates on the electrocatalyst surface, which was directly associated with the improvement in the catalytic performance.[141] This finding is expected to inspire others to exploit more novel classes of alkali metal-mediated compounds as advanced electrocatalysts for water splitting.

3.2. Insights into the Improvement of Activity by Alkaline-Earth Metals

Similar to the alkali metals, the alkaline-earth metals (Mg, Ca, Sr, Ba) are very abundant in the earth's crust. They are also known to be less harmful to humans and the environment and much more cost-effective as compared to noble metals. Moreover, compounds of these metals possess strong Brønsted basicity and a significant Lewis acidity, which can be ascribed to the low electronegativity of the metal ions and stable oxidation state to form covalent bonds with anions. Hence, albeit the alkaline-earth metals are usually not considered as catalytically active sites, the intriguing economics and chemical properties of the alkaline-earth metals are both interesting and promising for being incorporated into NNTM-based electrocatalysts for water splitting. According to the current research progress, the alkaline-earth metals are basically introduced into NNTM-based oxides to modify their OER and/or HER activity.[142–167]

Furthermore, the incorporation of alkaline-earth metals mainly leads a fundamental role in the following four aspects.[145–165] i) Tuning the alkaline-earth metal species in certain oxides can create lattice defects, which dictates a high conductivity and optimized free adsorption energy toward oxygen intermediates; ii) the alkaline-earth metal species can gradually leach from the catalysts during catalysis, which will in situ leave pores in the phase reconstructed NNTM-based (oxy)hydroxides catalysts, conducing to the exposure of active sites; iii) they mediate the formation of NNTM-species with high oxidation state, thus resulting in the improvement of catalytic activity; and iv) the incorporation of some alkaline-earth metal species into NNTM-based phase can alter the morphology during synthesis, such as nanosheet, which is beneficial for the accessibility of reactants to surfacial NNTM sites during catalysis. Taking the perovskite oxides (typically, ABO_{3-x} with alkaline-earth/rare-earth metal on the A-site and 3d-metal cations on the B-site, herein focuses on the discussion of alkaline-earth metal on the A-site) as an example, Bockris and Otagawa first reported their intrinsic electrocatalytic activities in 1984.[146] Since then, a series of perovskite oxides were intermittently studied as electrocatalysts for OER. However, these early studies only focused on the role of B-site because the e_g-filling status of B-site metal ions (e.g., Mn, Co, and Ni) had been demonstrated to be critical for high electrocatalytic OER activities by both the experimental and theoretical analysis.[147–149] In the last couple of years, researchers paid attention to A-site atoms and found that the A-site atoms could also play an indispensable effect in improving the OER activity.[150–155] Keeping this in mind, Hona and Ramezanipour found that upon gradually changing the Ca/Sr ratio from 1:0 to 0:1, abundant oxygen-deficiencies were created in perovskite oxide $Ca_{2-x}Sr_xFe_2O_{6-\sigma}$.[150] These deficiencies were beneficial for the improvement of the electrical conductivity of the compound, greatly expediting the charge transfer during catalysis, and thereby enhancing OER activity in the alkaline media. Further study by Sankannavar and Sarkar found that the partial substitution of trivalent La by bivalent Ca not only creates much more oxygen vacancies in $La_{1-x}Ca_xFeO_{3-\sigma}$, but also increase the average oxidation state of iron from Fe^{3+} to Fe^{4+}, boosting the reaction kinetics for OER alkaline media.[151] Remarkably, Shao and co-workers found that the optimized $Ba_{0.5}Sr_{0.5}Co_{0.8}Fe_{0.2}O_{3-\sigma}$ (BSCF) combined with the NiO amorphous layer enabled up to more than 300-fold enhanced mass-specific OER activity compared to the crystalline $Ba_{0.5}Sr_{0.5}Co_{0.8}Fe_{0.2}O_{3-\sigma}$ bulk phase in the alkaline electrolyte.[152] Further insightful research by Schmidt and co-workers claimed that after a period of OER, an amorphous CoFe (oxy)hydroxide layer was generated on the surface of $Ba_{0.5}Sr_{0.5}Co_{0.8}Fe_{0.2}O_{3-\delta}$ in the alkaline media (**Figure 6**A), which was further verified by the significant Co K-edge shift by XAS, proclaiming the change of CoO_6 coordination model from octahedral corner-sharing to edge-sharing.[153] In general, the leaching of both A and B-site atoms occurred during OER in the alkaline media, while B-site atoms would be redeposited onto the surface of the catalyst by the electrochemical-driving force.[153–155] When the redeposition rate was faster than the leaching rate, phase reconstruction would be clearly identified (Figure 6B).[154] However, because the leaching rate of A and B-site atoms was usually faster than the redeposition rate in acidic media, the phase reconstruction was hard to be observed
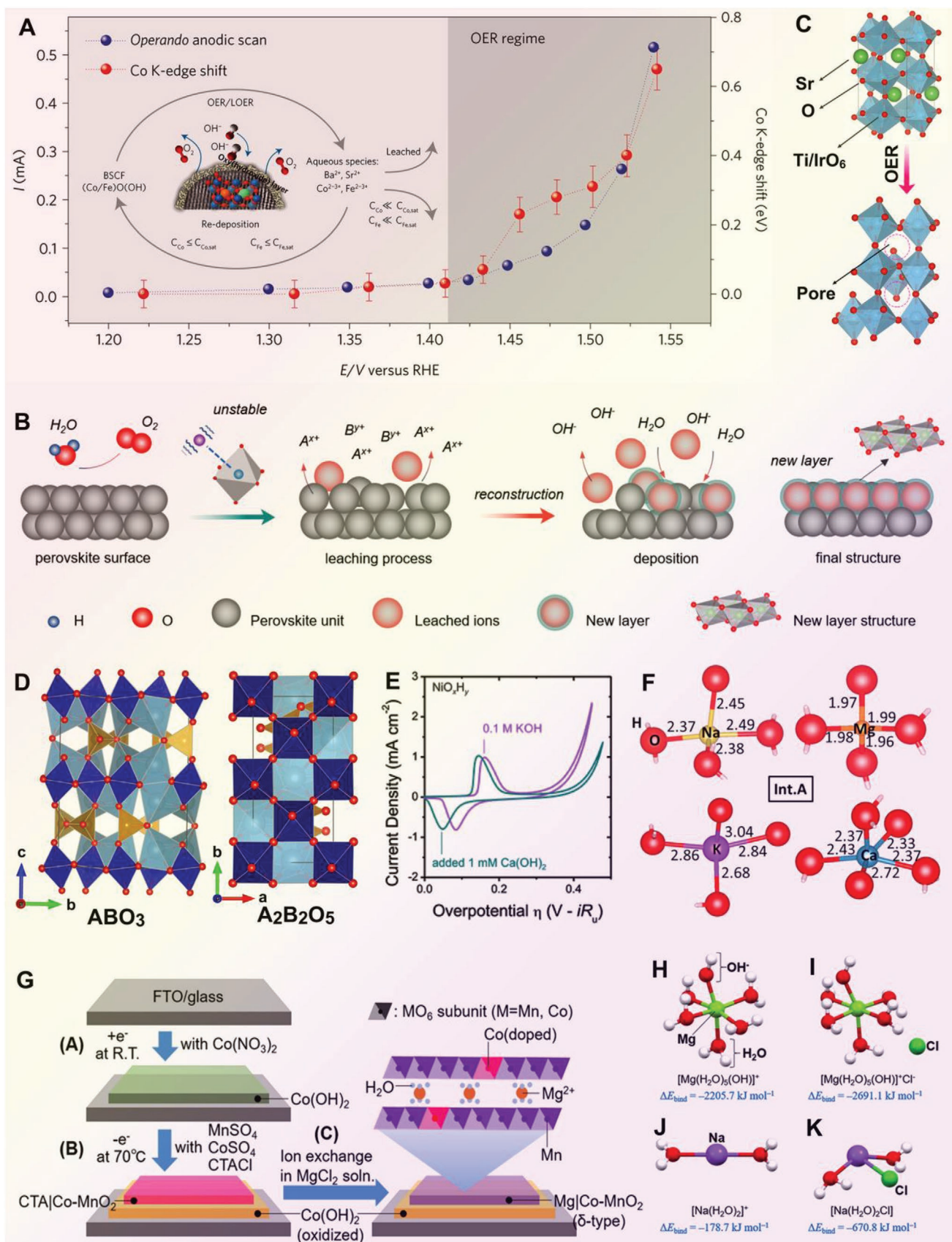
for the ABO_3 phase during acidic OER.[156–160] Nevertheless, the popularly observed alkaline-earth atoms leaching was also advantageous to the improvement of OER activity in this case. For instance, Zou and co-workers in situ created the IrO_2 onto the surfaces of $SrTiO_3$–$SrIrO_3$ solid solution, which showed an order of magnitude higher OER activity than pristine IrO_2 in acidic media. Further research found that the Sr species in $SrTiO_3$–$SrIrO_3$ support was very easy to be leached out during OER, which led to the formation of the porous structure to promote the OER activity (Figure 6C).[156] These findings well verified the elastic manipulation of alkaline-earth metal atoms in promoting catalytic activity.

The law of phase reconstruction in the alkaline media seems more appropriate to be applied to perovskite oxides with other chemical proportions, e.g., $A_2B_2O_5$-type. As it is well-known that the perovskites ABO_3 structure is constructed by BO_6-units corner-sharing octahedra with A cations located in the interstitial spaces. The $A_2B_2O_6$-type structure is one form of super-structures of the perovskites in crystallographic order.[159] One of the typical oxygen-deficient structures of this $A_2B_2O_6$-type is $A_2B_2O_5$ whose configuration belongs to the Brownmillerite-type structure (Figure 6D).[162] The lattice correlation between Brownmillerite and perovskite can be described in the following transformation: $a_b \rightarrow 2^{1/2}a_p$, $b_b \rightarrow 4a_p$, $c_b \rightarrow 2^{1/2}a_p$.[160,162] Yang and co-workers were the first ones to examine the OER activity of $Ca_2Mn_2O_5$, and found that it showed higher OER activity in the alkaline electrolyte than that of $CaMnO_3$, demonstrating its promising application in OER.[161] Inspired by this discovery, Habazaki and co-workers further examined the OER activity of Ca_2FeCoO_5 in 4.0 M KOH and proposed that the Ca species was leached out and also corroborated that Ca_2FeCoO_5 underwent crystalline-to-amorphous (CoOOH) phase transition during OER and adequately activated catalytically active domains, thus enhancing the OER activity.[162] Similar phase reconstruction was also observed in $PrBaCo_2O_{5+\delta}$ and novel $Ba_{0.5}Sr_{0.5}Co_{0.8}Fe_{0.2}O_{2+\delta}$.[163] Note that most of these perovskite oxides are still suffering from poor HER activity (usually more than an overpotential of 400 mV at the current density of 10 mA cm^{-2}).[164,165]

On the other hand, in light of the finding that the insertion of alkali-metal into the NNTM-based oxyhydroxide can improve the OER activity, Toroker and co-workers also examined whether the insertion of alkaline-earth cations could also improve the OER activity of Ni(Fe)OOH.[133] Unfortunately, they observed that Mg and Ca suppressed the catalytic activity (Figure 6E). This is mainly because of the strong affinity of alkaline-earth cation toward O atoms from the electrolytes that can strongly bind to water and other OER intermediates, disturbing the interlayer network of water molecules, and hence inhibiting effective interaction with surface intermediates (Figure 6F). This could explain why electrolytes endowing with a weak acidity by alkali metals are preferable for OER. Moreover, the unfavorable size of the interlayer species caused by the strong interaction between alkaline-earth metals with oxygen also significantly degrade the adsorption ability and stability of key reaction intermediates, and thus increasing overpotential values. Nonetheless, the insertion of alkaline-earth metal (e.g., Mg) ions has been demonstrated to be beneficial for the selective oxygen evolution from chloride-containing water or seawater.[166,167] For instance, Nakayama and co-workers reported that the intercalation of Mg into Co-doped δ-type (layered) MnO_2 (Mg|Co–MnO_2) by ion-exchange boosted the OER activity of α-Co(OH)$_2$ when it covered on to the α-Co(OH)$_2$ (Figure 6G) and preferentially yielded oxygen with a Faradaic efficiency up to 79% even in the presence of chloride ions at 0.5 M of high concentration.[167] This could be owing to the fact that the Mg|Co–MnO_2 layer effectively blocked the permeation of Cl$^-$ and only allowed the penetration of H$_2$O and O$_2$, while the under α-Co(OH)$_2$ acted as an oxidation catalyst for the penetration of H$_2$O through the layer coating. Remarkably, although the blocking effect against Cl$^-$ decreased in artificial seawater (pH 8.3) due to the ion-exchange of the intercalated Mg^{2+} ions with Na$^+$ in solution, the OER efficiency still could be remained as high as 57%, much higher than that without the Mg|Co–MnO layer (28%). DFT calculations further unveiled that the most stable structure of hydrated Mg^{2+} ion, in which a part of coordinated H$_2$O molecules was hydrolyzed, possessed less affinity toward Cl$^-$ than that of hydrated Na$^+$, thus blocking Cl$^-$ more effectively than Na$^+$ (Figure 6H–K). This also demonstrated that Mg modified the interlayer spaces between MnO_2 layers acted as pathways for H$_2$O molecules to reach the active sites of the underlying Co(OH)$_2$. Since seawater splitting is currently a hot topic in the water splitting field,[168–170] we anticipate that the SPFM species could be applied in the related field and the alkaline-earth metal-mediated oxides may be very promising.

3.3. Insights into the Improvement of Activity by Rare-Earth Metals

Rare-earth metals consist of Y, Sc, and other 15 lanthanide elements, located near to the alkaline-earth metals. Because the electron orbitals of the lanthanoid elements are similar to those of the alkaline-earth metal elements, the chemical properties of compounds containing the lanthanoid metals are close to those

Figure 6. A) Current and shift of the Co K-edge position recorded during an anodic polarization of the BSCF electrode. Inset in A): a self-assembled active surface layer induced by OER/LOER and dissolution/redeposition mechanism. Reproduced with permission.[153] Copyright 2017, Nature Publishing Group. B) Schematic diagram of perovskite surface reconstruction. The gray balls represent the unit of perovskite structure, while the pink ball and the ball with a cyan layer represent the leached ions and hydrated ions, respectively. Reproduced with permission.[154] Copyright 2021, American Chemical Society. C) Structure of SrTi/IrO$_3$ before and after OER. Reproduced with permission. D) Crystallographic structure of the ABO$_3$ and brown-millerite-type A$_2$B$_2$O$_5$ compound with a 57 Pbcm symmetry. Reproduced with permission.[162] Copyright 2019, American Chemical Society. E) Linear sweep voltammetry curves of NiO$_x$H$_y$ in 0.1 M KOH before and after the addition of 1 × 10^{-3} M Ca(OH)$_2$. F) Bond distances (in Å) for molecular clusters formed by electrolyte species and surrounding O atoms that exist in the interlayer space of NiOOH. Reproduced with permission.[133] Copyright 2017, American Chemical Society. G) Schematic flow diagram to construct the bilayer structure composed of Mg-intercalated δ-MnO$_2$ doped with Co (upper) and Co(OH)$_2$ (below). H–K) Stable structures of hydrated (H,I) Mg^{2+} and (J,K) Na$^+$ ions associated (H,J) without and (I,K) with Cl$^-$ based on DFT calculations. Reproduced with permission.[167] Copyright 2020, American Chemical Society.

**ADVANCED
SCIENCE NEWS**

www.advancedsciencenews.com

**ADVANCED
MATERIALS**

www.advmat.de

containing the alkaline-earth metals to some extent.[171] Typically, both the rare-earth metal and alkaline-earth metal can be used to construct the metal perovskite oxides, and they exhibit similar mechanisms in promoting the OER activity, such as the creation of the oxygen-vacancies, enhancement of the intrinsic catalytic activity, generation of the porous structure by leaching, as well as the acceleration of the dynamic reconstruction of active phase during OER.[172–176] Since the discussion on the role of alkaline-earth metals in perovskite oxides has already been presented, only limited essential details on rare-earth metals have been provided here. In fact, there are two notable factors while determining the catalytic activity of these materials and require considerable attention. The first one is that no matter what the rare-earth metal-based perovskite oxides or the alkaline-earth metal-based ones are, those which can concurrently undergo the metal leaching and phase reconstruction during OER usually exhibit the admirable catalytic activity (**Figure** 7A).[154] The other is that the OER activity might be highly dependent on the atomic radius of rare earth metal, that is, the OER activity initially increased and then decreased with the gradual decrease of average atomic radius (Figure 7B).[177] Moreover, because the atomic radius for rare-earth metal is larger than those for alkaline-earth metal, and thus hard to directly insert them into the layer of the NNTM-based (hydro)oxide or oxyhydroxide, unlike alkaline-earth metal ions. Nevertheless, rare-earth atoms can be doped into the host lattice of these NNTM-based compounds and their catalytic activity can then be effectively improved.[178–186] In this regard, Xu et al. revealed that upon doping the Ce atom into the NiFe-LDH, three benefits were identified to boost the OER activity.[178] First, it changed the layer composition and coordination structure of LDH by the formation of the eightfold dodecahedron or ninefold monocapped square antiprism coordination layers, second, since the doped Ce presented a mixture valence of Ce^{3+} and Ce^{4+}, lattice distortion, and imperfections of active metal sites were naturally generated and lastly, a certain number of oxygen vacancies were formed to maintain the charge balance. Needless to say, all three factors were crucial to optimize the adsorption free energy during OER. In the meantime, Chai and co-workers doped the $Co(OH)_2$ nanosheets with Ce for efficient OER and revealed that the intimate interaction between Ce and Co species provided the "d–f electronic ladders" for accelerating electron transfer of the catalytic surface (Figure 7C).[181] These enhancement mechanisms can also be applied to several systems, such as NNTM sulfide,[183] phosphide,[184] high entropy oxide,[185] and metal–organic framework.[186]

Apart from the aforementioned function, rare-earth metals also display some other attractive functions:[71,187–195] i) alloying with other NNTMs to form the newly structured intermetallics with high conductivity, ii) binding with anions to serve as a confinement substrate to anchor the single metal atom, and iii) taking rare-earth element oxides or hydroxides as the coupling subunit to build heterointerfaces. On the basis of the Brewer–Engel theory,[187] alloying the NNTMs that have empty or half-filled vacant d orbitals with rare-earth metals with empty and vacant d orbitals is a viable strategy to design the advanced electrocatalysts for HER. Furthermore, according to the guidance of the Brewer–Engel theory, hydrogen storage materials such as intermetallic $LaNi_5$ with the highest symmetry of phase

structure and minimum entropy for HER is considered as one of the most active ones.[187] This observation was first reported by Miles while studying the HER activity of $LaNi_5$, which delivered an overpotential of about 100 mV at 2 mA cm^{-2} in 6.8 M KOH at 80 °C.[188] Soon after, Tamura et al. investigated the catalytic HER feature of several intermetallics including $LaNi_5$, $LaCo_5$, and $MmNi_5$ (mixed metal).[189,190] It was found that all of these intermetallics exhibited superior HER activity over the individual metals in the alkaline media, verifying the apparent synergistic effect between rare-earths and NNTMs. Moreover, it was proposed that the NNTM species were the dominant active sites because of their moderate binding ability toward H-intermediate. Hence, a Ni-rich surface would enhance the adsorption of the hydrogen atom at the electrode surface to improve electrocatalytic activity for the HER. In view of this, many have attempted to dope a small amount of rare-earth into NNTM. For example, various rare-earth elements such as Y, Ce, Pr, Sm, and Dy with low contents (usually <10 at%) have been adopted and demonstrated to be effective in promoting the HER activity of Ni, Fe, and/or Zn.[191–195] These findings are intriguing as the hydrogen storage materials $RENi_5$-type (RE = rare-earth) intermetallics are capable of catalyzing hydrogen production.

From the perspective of thermodynamics, the rare-earth metal oxide is the most stable phase which usually stabilizes in only one oxidation state and is chemically inert during the electrochemical reaction.[196] Nonetheless, many rare-earth metal oxides share a similar crystallographic system with many NNTM (hydro)oxides, oxyhydroxides, and chalcogenides.[197–199] Taking CeO_2 and NiO as an example, the theoretical lattice mismatch between them was found to be about 23%. Such a moderate lattice mismatch is expected to provide them with the possibility for the lattice coupling accompanied with the interfacial charge interaction, in which both the lattice mismatch and charge transfer are expected to accelerate the phase reconstruction from NiO to active NiOOH phase. On this account, Chen and co-workers recently achieved a pseudo-periodical coupling of Ce–O lattice with Ni–O lattice in ultrathin heteronanowire arrays for efficient OER.[71] The results found that CeO_2 could not only build a lattice coupling with the NiO, being in favor of the generation of abundant O-vacancies and thereby an acceleration of deep phase reconstruction from NiO to NiOOH but also the pseudo-periodical arrangement manner ensured the split of NiO into accessible NiOOH nanodomains without aggregation, facilitating the utilization of active sites and diffusion of mass. More importantly, the CeO_2 could be well coupled with the in situ formed NiOOH and implemented the charge injection, and thereby an optimization of the reaction free energy for oxygen-intermediates (Figure 7D,E). Owing to these traits, when functioning as a (pre)catalyst in 1.0 M KOH, it exhibited much better OER activity than bare NiO and commercial IrO_2-based electrocatalyst. Several encouraging findings also revealed that the appropriate coupling of rare-earth oxides could also inhibit the dissolution or corrosion of NNTM and lattice oxygen in the electrolyte.[200–202] Tang and co-workers demonstrated that the protection of the CeO_x layer could remarkably suppress the dissolution and loss of oxidized Co species in CoS, which improved the OER durability.[201] Obata and Takanabe compared the OER behavior between $NiFeO_x$ and CeO_x layer-coated $NiFeO_x$, and they observed that $NiFeO_x$

ADVANCED
SCIENCE NEWS

www.advancedsciencenews.com

ADVANCED
MATERIALS

www.advmat.de
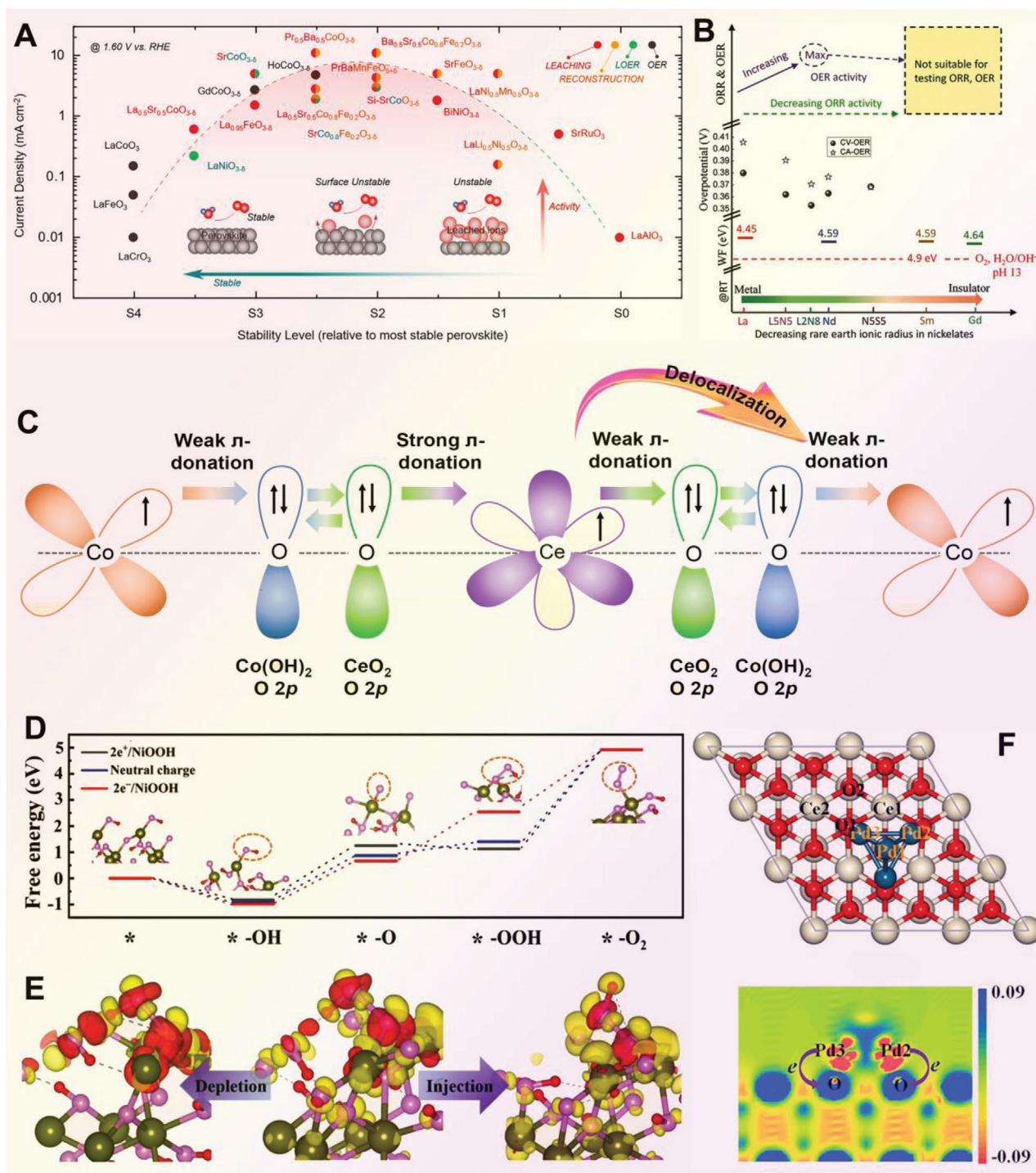
Figure 7. A) The summarization of a series of perovskite-type oxides for the stability level and OER current density at 1.60 V versus RHE by Li and co-workers. The dashed volcano lines and filling are shown for guidance only. Reproduced with permission.[154] Copyright 2021, American Chemical Society. B) Schematic illustration of the trends in the conductivity, the work function (WF) values, the OER overpotential to obtain 40 μA cm^{-2} at pH 13 with decreasing rare-earth ionic radius in nickelates. Reproduced with permission.[177] Copyright 2018, Wiley-VCH. C) Schematic representations of the electronic coupling among Co, Ce, and O 16 in Ce$_{0.21}$@Co(OH)$_2$. Each arrow indicates one electron with spin direction. Reproduced with permission.[18] Copyright 2021, Elsevier. D) Free energy landscape for OER on (101) facet of NiOOH under different charge doping. E) Absorption structure and charge density redistribution between intermediate OOH and NiOOH with different charge doping states. The yellow isosurface reflects the charge gaining region, while the dark red isosurface reflects the charge losing region, respectively. Reproduced with permission.[71] Copyright 2021, Wiley-VCH. F) Top view of Pd$_4$@CeO$_2$ model and the possible adsorption sites for H* on the Pd$_4$@CeO$_2$. The charge density difference $\Delta\rho$ of the Pd$_4$@CeO$_2$ model for the slice (vertical to the surface of substrate CeO$_2$) cut along the Pd$_2$–Pd$_3$ bond, where the red and blue areas denote the decreased and increased electron densities, respectively. Reproduced with permission.[205] Copyright 2019, American Chemical Society.

**ADVANCED
SCIENCE NEWS**

www.advancedsciencenews.com

**ADVANCED
MATERIALS**

www.advmat.de

gradually lost activation due to the dissolution of active Fe sites into solution.[202] However, with respect to the CeO_x layer-coated $NiFeO_x$, both the catalytic OER activity and stability were well maintained. This is owing to the fact that the CeO_x layer possessed a unique perm-selectivity where the O_2 and OH^- were allowed to permeate whereas the diffusion of redox ions such as Fe^{n+} was prohibited to permeate, thus hindering the dissolution of $NiFeO_x$ core.
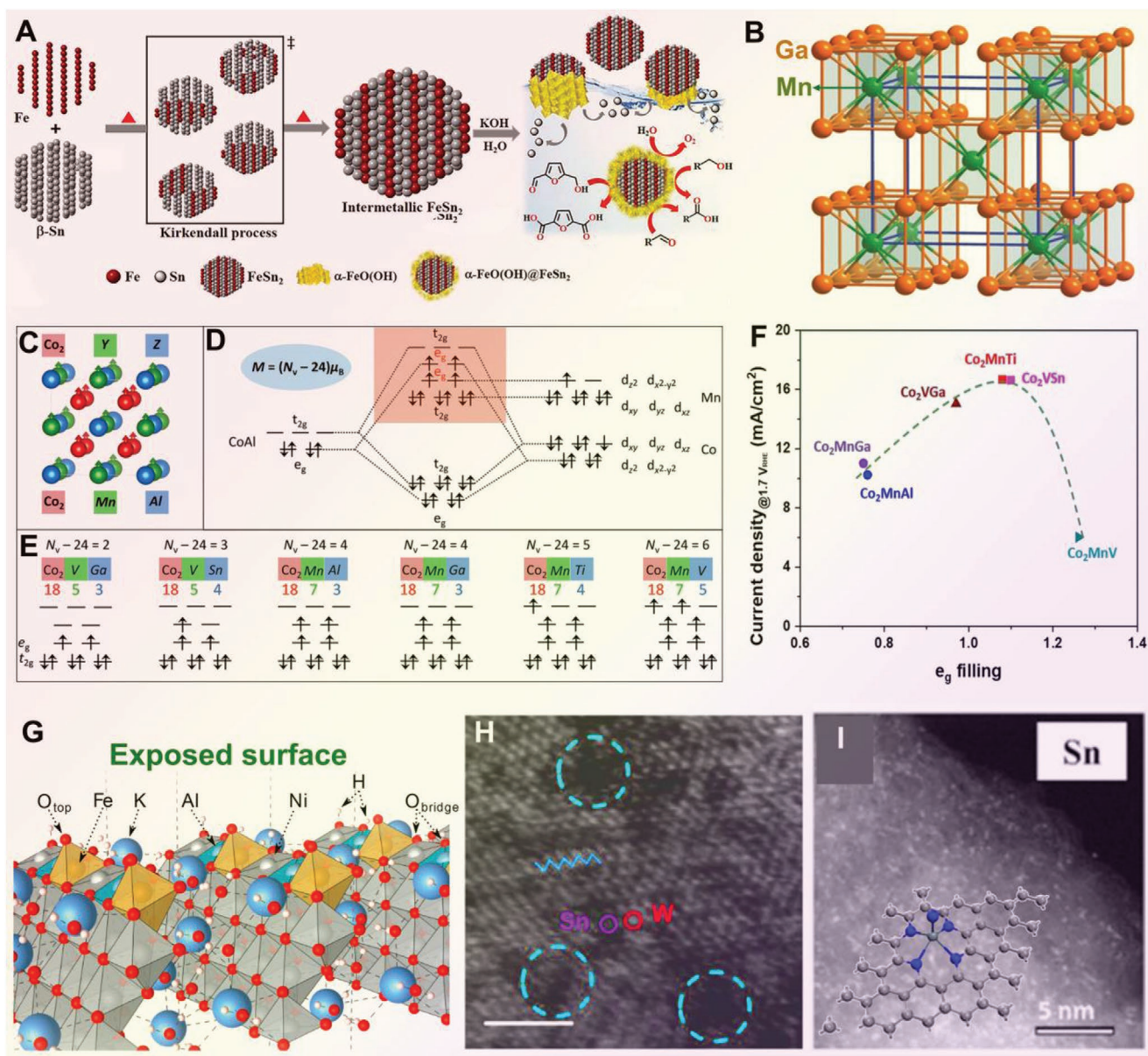
In consideration of the extremely high chemical stability against the electrochemical process, the rare-earth metal oxide is also capable of serving as the ideal matrix to confine the single atom or cluster for electrocatalysis.[203,204] Recently, Chen and co-workers anchored sub-nanometer-sized Pd clusters onto the porous CeO_2 rods via a convenient wet chemical method.[205] The theoretical calculation revealed that compared to the bare Pd nanoclusters, the electron transfer between Pd and CeO_2 (Figure 7F) could effectively modulate the adsorption state of H* on the subunit of the Pd cluster, and this effect strikingly promoted the HER catalytic activity with ultralow onset overpotential of 36 mV and maintained the industrial-scale large current density even after 10 000 cycles. Although this work focused on the rare-earth metal oxide-supported precious metal nanocluster, the finding is expected to encourage the further pursuit of the synthesis of rare-earth metal oxide-supported isolated atomic NNTM as well as its application in water splitting.

3.4. Insights into the Improvement of Activity by Lean Metals

Compared with transition metals, lean metals which are located in the basic metal region (Figure 1) have higher electronegativities, lower melting points, and boiling points, and are softer. However, lean metals are distinguished from "quasi metals" because of their much higher melting and boiling points than that of other main group elements in the same period. Moreover, their crystalline structures tend to show covalent or directional bonding effects, having fewer nearest coordination atoms than other metallic elements. Among these lean metals, those referred to Al, Ga, Sn, and Bi are usually utilized for the OER and HER catalysis, and they improve the OER and HER activity in terms of the following aspects.[103,105,206–231] i) These lean metals can be readily etched in both the alkaline and acidic solutions, generating beneficial results including the formation of pores and partial phase reconstruction. ii) They can be prone to hybrid with other metals to form the (ordered) intermetallics with high conductivity. iii) The addition of these metals can also shape the morphology of the resulting materials system. iv) The presence or the incorporation of these metals in the catalytic system can tune the vacancy and electronic structure. v) These lean metals-involved compounds do not only serve as a matrix for confining single atoms but also to evolve single atom for catalysis. Recently, Menezes et al. demonstrated a controllable synthesis of $CoSn_2$ nanocrystals as efficient bifunctional OER and HER electrocatalysts using the solution chemistry method.[206] It was found that under alkaline media, the leaching of Sn from the crystal lattices, and oxidation of Co furnished highly disordered amorphous active $CoO_x(H)$ on the surface of $CoSn_2$ for OER, while the Co^0 atoms in the $CoSn_2$

acted as active sites for HER. Meanwhile, the retention of partial intermetallic $CoSn_2$ structure ensured high electrical conductivity to accelerate the charge transfer. Encouraged by this finding, they further synthesized the intermetallic $FeSn_2$ for OER in the alkaline media and identified the in situ generation of core–shell-like α-FeO(OH)@$FeSn_2$ where α-FeO(OH) acted as the active site while $FeSn_2$ remained the conductive core, thus giving rise to a remarkable OER activity (**Figure 8**A).[207] Moreover, Menezes et al. explored $MnGa_4$ as a new material for electrocatalytic OER, in which $MnGa_4$ belongs to a d–sp bonded Hume-Rothery intermetallic compound with strong directional covalent bonds and metallic nature (Figure 8B).[68] It was found that it could show a better OER activity than that of commercial IrO_2 and other NNTM-based oxides/hydroxides. The higher activity has been associated with two factors: first, due to the in situ partial electroconversion to disordered and defect-rich MnO_x phases of α-Mn_3O_4, δ-MnO_2, and β-$MnOOH$ with abundant Mn^{3+} sites on the surface of $MnGa_4$. Second, due to the generation of porous active nanodomains by leaching of Ga, leading to a larger electrochemically active surface with a higher density of active sites, and fast electron transport from the catalyst surface and the electrode. In theory, compared to those NNTM (hydro)oxides, chalcogenides, and phosphides, the core formed by intermetallics shows a higher conductivity and results in a faster electron transfer. Motivated by these appealing results, more recently, Tüysüz and co-workers studied the OER activity of a series of the Heusler intermetallics such as Co_2MnAl, Co_2MnGa, Co_2VGa, and Co_2VSn which were synthesized by the arc-melting method (Figure 8C–E).[209] The leaching of Al, Ga, and Sn on the surface of these compounds could also be observed during OER. Furthermore, a strong volcano-like correlation between the e_g orbital occupancy of reactive Co sites and OER activity was found on these Heusler intermetallics, which governed the M–O bond strength and thus probably the tendency to phase reconstruction (Figure 8F). Importantly, the e_g orbital occupancy of Co active site could be precisely regulated by Al, Ga, and Sn in these compounds, which may provide the basis for a future design of this kind of lean metal-containing electrocatalysts.

Benefiting from the above advantages by the leaching of lean metals in the alloy, many lean metal-mediated catalytic systems were developed for OER such as NNTM sulfides,[210,211] selenides,[212] and phosphides.[213–215] However, it is surprising that no structural change or leaching after long-term OER test in alkaline media occurred in the lean metal-incorporated hydroxide probably due to their relatively higher thermodynamic stability.[105,216–200] Nonetheless, the free-adsorption energy toward oxygen-containing intermediates was optimized. For example, the Ga-doped FeNi-based hydroxide delivered an excellent composition and structure stability after 100 h of cycles during OER. Moreover, upon the doping of Ga, the energy barrier for the rate-determination step from the adsorption of OH^- to the adsorption of O^- was effectively decreased.[216] In addition, the doping with these lean metals into hydroxides could also induce an internal lattice strain, which could strikingly decrease the reaction barrier for electron transfer during OER.[217] Bent and co-workers also found that after the doping of Al into FeNi-oxyhydroxide, the nanosheet-like morphology was obtained, which helped to expose a larger number of active

2108432 (15 of 31)

**ADVANCED
SCIENCE NEWS**

www.advancedsciencenews.com

**ADVANCED
MATERIALS**

www.advmat.de

Figure 8. A) Schematic representation of the formation of structurally ordered intermetallic FeSn$_2$ as well as the substantial reconstruction at the surface under alkaline electrochemical reaction conditions. Reproduced with permission.[207] Copyright 2020, Wiley-VCH. B) Crystal structure (Mn: green; Ga: orange). Reproduced with permission.[68] Copyright 2019, Wiley-VCH. C) Crystal structure of Co$_2$YZ Heusler compounds. D) Illustration of molecular orbital diagram of Co$_2$MnAl. E) The magnetic moment and electron occupation of the selected Co$_2$YZ compounds. F) The volcano-shape plot of the OER activity, defined by the current density at 1.7 V versus RHE, against the occupancy of the e_g electron of Co in Heusler compounds. Reproduced with permission.[209] Copyright 2021, Wiley-VCH. G) The atomic structure of the (100) surface of γ-Ni-(Al)-FeOOH under OER conditions. The repeating unit cell explicitly shows the most active on-top Fe site (denoted as O$_{top}$) with Al as a surface neighbor. Reproduced with permission.[105] Copyright 2019, American Chemical Society. H) STEM image of metallic 1T′-Sn$_{0.3}$W$_{0.7}$S$_2$. Inset: yellow dotted line circles with some defects. Scale bar: 2 nm. Reproduced with permission.[218] Copyright 2020, Wiley-VCH. I) Structure of single-atom metals. Reproduced with permission.[221] Copyright 2020, American Chemical Society.

sites, thus led to a more than a threefold increase of TOF-normalized OER activity in alkaline media if compared to bare FeNi-oxyhydroxide (Figure 8G).[105] Importantly, many reported lean metal-tuned HER catalysts do not show any leaching under electrocatalytic conditions because their structures are remarkably stable.[218–220] The main aim of lean metal-doping for HER is to enhance the intrinsic electrical conductivity, lattice

distortion, and defects. By a combined experimental and theoretical investigation, Liu and co-workers revealed that when the metal-stable Sn$_{0.3}$W$_{0.7}$S$_2$ was formed based on WS$_2$, the crystal structure was converted from trigonal prismatic (2H phase) to distorted octahedral (1T′ phase) (Figure 8H).[218] Furthermore, the conductivity was also changed from semiconductor to metal while lattice distortion led to a large number of catalytic active

**ADVANCED
SCIENCE NEWS**

www.advancedsciencenews.com

**ADVANCED
MATERIALS**

www.advmat.de

sites. Impressively, the metallic $Sn_{0.3}W_{0.7}S_2$ phase exhibits a comparable HER activity to Pt/C in 0.5 м H_2SO_4, together with outstanding stability after 3000 cycles. Note that the variation between Sn and W could also trigger the morphology variation. Recently, Peter and co-workers synthesized the novel ternary $Ni_3Bi_2S_2$ phase with monoclinic structure, which bears much better hydrogen adsorption and desorption ability than that of NiS owing to the localized charge-transfer between Ni and Bi, which facilitates the downward shift of the d-band center, thereby improving the catalytic activity.[219] All of the results mentioned above verify the crucial role of lean metals in improving both HER and OER activity.

As a matter of fact, like the rare-earth metal oxides, the lean metal oxides were also recently explored because they can serve as a substrate to confine single metal atoms. It is well-known that most of the reported single atom electrocatalysts are prepared on carbon-based supports, which integrates many advantages including high specific surface area and doping flexibility.[220] However, these carbon-based supports are prone to degradation due to corrosion and decomposition under harsh oxidizing conditions. To overcome this drawback, by a subsequent adsorption–calcination method, Coperét and co-workers successfully synthesized the SnO_2 matrix-confined single indium atom system, which showed a robust feature.[103] This may open a new viable way to optimize single atom electrocatalysts. Based on this, in order to further clarify whether a single lean metal atom itself has catalytic activity, Dou and co-workers developed a general cation-doping strategy to fabricate carbon-supported a series of single lean metal atoms (e.g., Bi, Sn) (Figure 8I).[221] However, both the experimental and theoretical calculation proclaimed their poor HER activity. Although this performance was not satisfactory, further optimization via electronic engineering or coordination engineering toward a single lean metal atom is expected to revive the catalytic activity.

3.5. Insight into the Improvement of Activity by Metalloids

Near to the lean metals, the metalloids (or semimetals) represent a series of main-group elements in the periodic table with similar electronegativity, which is larger than those of the main-group metals but lower than nonmetals. They often behave as electron donors toward nonmetals and as electron acceptors toward metals, giving rise to different classes of compounds with ionic, covalent, or metallic character. The metalloids for tuning the HER and OER activity usually encompass B, Si, Ge, As, Sb, and Te. Since the effects of Te have also been discussed in previous literature,[232,233] herein we focus on B, Si, Ge, As, and Sb as a component. Actually, the purpose of a metalloid in electrocatalysts for water splitting is somewhat related to the role of a lean metal:[234–242] i) the metalloid is a key component to form intermetallics, which transform into a core–shell architecture for efficient catalysis during the OER process; ii) doping of the catalyst with a metalloid can induce an oxygen vacancy, which then alters the catalytic mechanism and/or regulates the free adsorption ability during catalysis; iii) some of the metalloid-based compounds can function as an effective support to confine specific cluster formation and single atoms; iv) some of the metalloids can also be prepared in the form of single

atoms and can serve as the catalytic active sites to catalyze the HER; v) some metalloids possess a unique photothermal effect, i.e., it can effectively absorb the light and lead to the increase of temperature for the local part of electrocatalyst), which can boost the catalytic kinetics. In consideration of the above points, Driess and co-workers recently synthesized a series of intermetallics consisting of Fe or Ni and metalloids (Si, Ge, As) for OER using the single-source molecular precursor approach and arc-melting method.[234,236,237] All of these compounds were converted into active (amorphous) oxide surface-coated intermetallics during OER, accompanied by the dissolution of metalloids from the surface of the respective intermetallic compound, which was due to the fact that the covalent character of the metal–metalloid bonds has a tendency to be imparted in contact with the electrolyte (as predicted from Pourbaix diagram). Taking NiGe as an example, the original phase was completely converted by electrocorrosion to γ-NiOOH phase during OER.[237] Notably, owing to a large interlayer spacing of 7.0 Å hosted in γ-NiOOH that allowed the ionic intercalation of OH^- or CO_3^{2-}, a larger number of active sites for the OER become accessible. Moreover, compared to the directly synthesized γ-NiOOH, the in situ derived structure possesses more defects, higher ECSA, and better electronic conductivity, thus leading to superior OER kinetics and an expedited charge transfer to facilitate OER (**Figure 9**A,B). At the same time, Schuhmann and co-workers investigated the OER activity of a series of intermetallics by alloying Ni with metalloids (B, Si, As, and Te) in alkaline media.[228] The latter study confirmed again that surface Ni atoms were oxidized to NiOOH during the OER, which was the active phase of the catalyst. Furthermore, it was found that the metalloids were not completely leached out of the structure, rather a fraction of metalloids was oxidized to the corresponding oxoanions on the surface that tuned the interfacial electrode/electrolyte properties. For instance, the formed tetrahydroxyborate anion ($[B(OH)_4]^-$) during OER for Ni–B alloy showed Arrhenius basicity and was therefore believed to suppress the affinity and adsorption of OH^- before initiating the OER reaction, resulting in reduced kinetics of the hydroxylation reaction step observed for the NiB (pre)catalyst. Nevertheless, borate anions can noticeably improve the OER activity in both neutral electrolytes and alkaline electrolytes upon the initiation of OER, where they can act as proton acceptors to facilitate the rapid electron and proton equilibrium between Ni–OOH and Ni–O_2 states.

As previously claimed in reports, one can dope NNTM-based catalysts with SPFMs and these metallic species can perform very well when combined with oxides.[229–232] In such oxides, a dynamic phase reconstruction can easily be triggered during OER when the metal leaching rate is slower than that of the metal deposition. In oxides, oxygen vacancies always exist, which sometimes leads to another possible catalytic mechanism, namely, the LOM, which is different from the above-mentioned AEM.[233,235] The LOM mechanism is involved with a direct participation of oxygen anions from the lattice as an active intermediate in the OER, which is supported by ^{18}O isotope labeling experiments of the reaction product as well as DFT calculation.[243–248] Shao and co-workers reported that the incorporation of tetrahedral Si into octahedral Co sites of strontium cobaltite perovskite enables the generation of oxygen vacancies
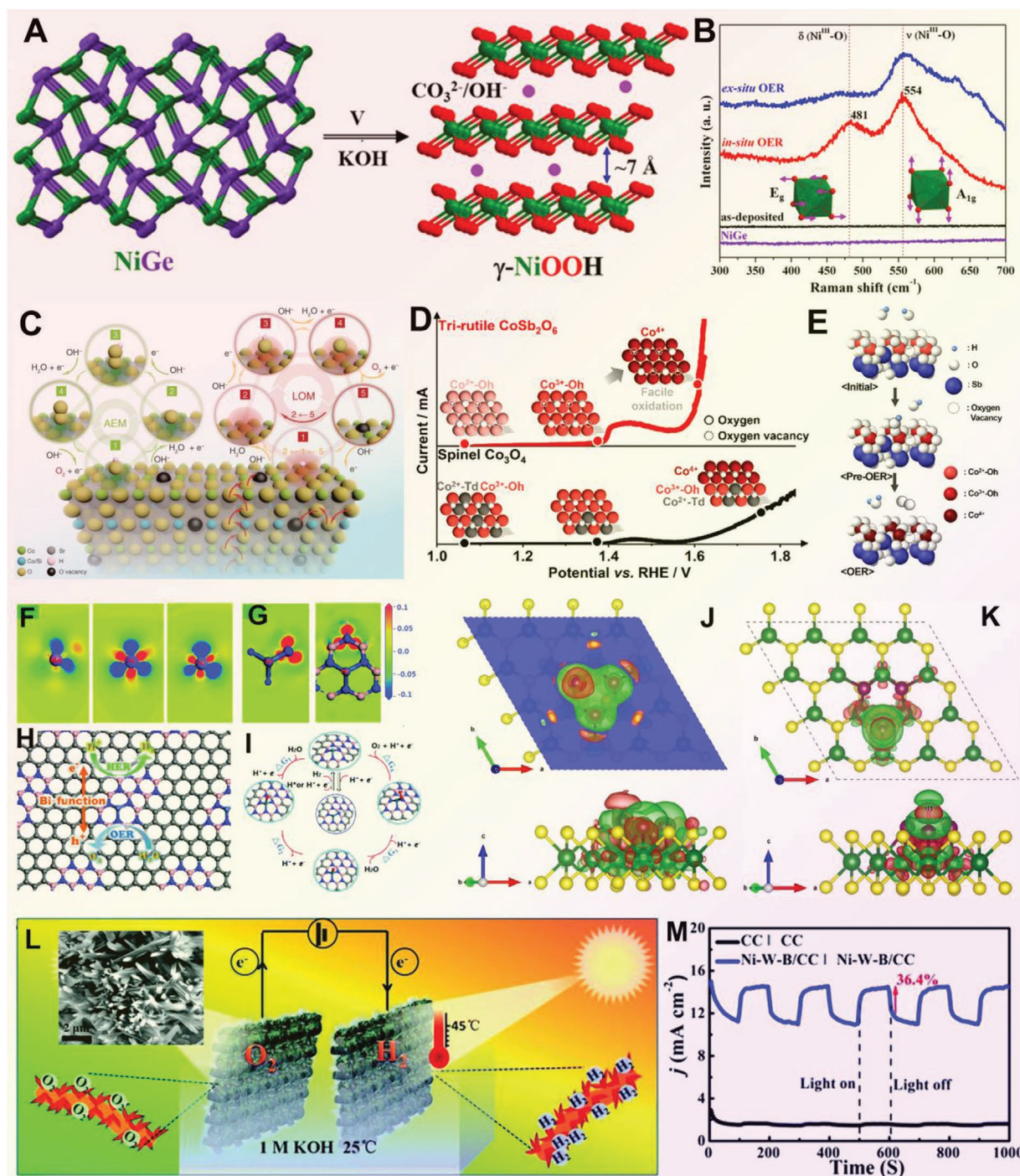
Figure 9. A) crystal structure of NiGe and electrochemically generated γ‑NiOOH with ionic intercalation of OH^-/CO_3^{2-} during OER in an alkaline KOH electrolyte. B) Quasi in situ and ex situ Raman spectroscopy of NiGe (OER CA, 24 h). Reproduced with permission.[237] Copyright 2021, Wiley-VCH. C) A schematic illustration of the AEM and LOM reaction pathways on Si-incorporated strontium cobaltites. Reproduced with permission.[238] Copyright 2020, Nature Publishing Group. D) OER behavior of $CoSb_2O_4$ and Co_3O_4 and E) proposed scheme during the increasing potential for the OER of $CoSb_2O_4$. Reproduced with permission.[256] Copyright 2021, American Chemical Society. Slices of the distribution of exchange/polarized charges of F) NNTM or G) N atoms in NNTM@BCN1. Slices are parallel to the nanosheet and across the considered atom. H) Schematic of NNTM@BCN as a bifunctional catalyst of overall water splitting. Efficient electron–hole separation supports that the single atom catalyst may present high activity for OER, with the N atoms being highly active sites for HER. I) Elementary steps of OER and HER displaying the structures of the adsorbed species *H, *OH, *O, and *OOH. Reproduced with permission.[258] Copyright 2019, The Royal Society of Chemistry. The top view and side view of the 3D charge density difference plots for $Ge_3@MoS_2$ J,K) H-adsorbed $Ge_3@MoS_2$-H. Reproduced with permission.[259] Copyright 2021, Elsevier. L) Schematic illustration of the photothermal coupling of Ni–W–B/CC electrode. M) The current density–time curve of the water splitting device under PTE. Reproduced with permission.[260] Copyright 2019, The Royal Society of Chemistry.

as well as reduces the bulk oxidation state of Co.[238] Benefiting from this, it exhibited a tenfold improvement of intrinsic OER activity owing to more than tenfold enhancement in oxygen diffusivity. Such an oxygen diffusivity enhancement changed the conventional adsorbate evolution-dominated mechanism into a lattice oxygen oxidation-dominated mechanism (Figure 9C). This is because, upon the initiation of OER, the lattice oxygen evolved at the surface will be quickly replenished by oxygen ions diffusing from the bulk of the electrocatalyst. Of note, even the LOM mechanism dominated in this perovskite, the surface reconstruction was also triggered while a constant dissolution/deposition process guaranteed the stability. Moreover, the LOM mechanism can also occur for several other types of oxygen-containing OER catalysts, for example, spinel oxide,[249] oxyhydroxide,[250] and phosphate.[251] In addition, the doping of metalloids into oxide compounds will generate other following merits.[242,243] First, metalloids could be used to grasp electrons from NNTM and transfer them to neighboring oxygen atoms in the oxides owing to their moderate electronegativity (1.9–2.1). Thus, electron-enriched or -depleted local regions can favorably be generated on the surface of oxides, which may be beneficial for maximizing the number of active sites for electrocatalytic water splitting. Second, electronic coupling interactions between metal d-orbitals and metalloid sp-orbitals can shift the center of the d-orbital from the Fermi level, leading to an increased conductivity of the oxide. In fact, metalloids can also be used as a component to form novel compounds with abundant anion vacancies for catalysis; whose catalytic behavior is similar to those of related lean metal-containing ones.[244–255] For instance, Lee and co-workers reported the trirutile $CoSb_2O_6$ with octahedral Co^{2+} sites and inactive Sb^{5+} ions as an OER electro(pre)catalyst in the alkaline media.[256] In situ XAS results showed that the oxygen vacancy in $CoSb_2O_6$ improved the OH^- adsorption kinetics by tuning the low oxophilicity of the Co atom, and it facilitated the further complete oxidation of Co^{3+} to the real active Co^{4+} site for OER, that is, reaching an overall higher oxidation state of Co than in spinel-type Co_3O_4 (Figure 9D,E).

Metalloids-containing compounds may be one promising support to confine single metal atoms for efficient catalysis.[257,258] For instance, Jiang and co-workers proposed a novel theoretical design of a nickel single atom catalyst (Ni-SAC) supported by a hybridized graphene–boron nitride monolayer (BCN), for a highly active bifunctional electrocatalyst for both HER and OER (Figure 9F–I).[258] As the B-vacancy defects on BCN can immobilize Ni-SACs with high diffusion barriers, and owing to the effective charge polarization and synergistic effects of components, this Ni-SAC exhibited remarkable electrocatalytic activity with very low overpotentials of 20 and 470 mV for HER and OER, respectively. Intriguingly, in $Ge_3@MoS_2$, the Ge atoms act as electron donors toward MoS_2 and increase its conductivity.[259] The unique coexistence of electron-poor and electron-rich regions near the Ge atoms enables the adsorption of "free" H radicals (Figure 9J,K) for which the barrier is even lower than that of the commercial Pt/C catalyst. The latter work is expected to stimulate more research toward optimization of other 2D materials through doping with metalloids for efficient HER. In line with that, Dou and co-workers could confirm a high HER activity using *N*-doped carbon-supported single Ge

atoms in a combined theoretical and experimental investigation.[221] In addition to the aforementioned functions, a local photothermal effect (PTE) was observed in some metalloid-mediated NNTM-based electrocatalysts. Guo and co-workers synthesized a series of borides based on the Ni–W–B system and demonstrated that the reaction kinetics of both HER and the OER can be accelerated by external light illumination of the working electrode (Figure 9L,M).[260] Upon the injection of light, the overpotentials of a PTE-coupled Ni–W–B/CC electrode at 100 mA cm^{-2} in the alkaline electrolyte were decreased by 35 and 23 mV for HER and OER, respectively. Remarkably, this PTE-coupled electrode enabled an overall water splitting device with a current density of 25 mA cm^{-2} at an ultralow cell voltage of 1.524 V, ranking in the top performance among the recently reported SPFM-mediated electrocatalysts. This discovery may initiate more research on using metalloids such as Bi to feature an intrinsic photothermal effect for effective water splitting. **Table 2** summarizes the most recent research trends in using SPFM-mediated electrocatalysts for advanced water splitting systems. Most of them show an intriguing catalytic activity and will stimulate a knowledge-based design of improved systems for overall water splitting. Note that high stability is indispensable to the practical application of low-cost non-noble metal-based electrocatalysts for water electrolysis. Because the development of SPFM-mediated catalysts has just received particular attention in very recent years, the systematical report on whether and how SPFM species can improve the stability of transition metal-based catalysts is still insufficient. Motivated by this point, we tried our best to survey the related literature, and as expected, some reports confirm that SPFM species could play a positive role in enhancing the stability of NNTM-based electrocatalysts. To highlight the operation stability, we have now also added the durability at large current density for SPFM-mediated NNTM-based electrocatalysts toward water splitting in Table 2. Remarkably, nearly all these electrocatalysts showed outstanding stability. Moreover, several comparative works substantiated that the NNTM catalysts containing SPFM species could stabilize their robust catalytic capability in HER, OER, and overall water splitting with less deactivation, compared with the associated pristine NNTM or directly synthesized NNTM-based (oxy)hydroxides.[136,225,236,261,262] The high operation stability should be closely related to the chemical and structural stability of the electrocatalyst. As it is well-known that the chemical stability of active NNTM species is vital for the long-term application of NNTM-based catalysts, the easy leaching of the active TM during water splitting has already been verified, especially the Fe species in the benchmark NiFe-based OER catalysts.[263,264] Recently, the incorporation of SPFM species (e.g., metalloid borates) into alkaline electrolytes has been shown to contribute to maintaining the OER durability of NiFeCo-based (oxy)hydroxides. As the presence of borates in the electrolyte can increase the Fe solubility of the catalysts, they can conversely promote the redeposition of Fe from the electrolyte, reaching the dissolution–redeposition equilibrium, and accordingly can facilitate to elevate the chemical stability of active NNTM species.[265] However, two questions are still unclear and have not been addressed in the current publications: i) which incorporation manner does the SPFM species can better prevent the chemical loss of active NNTM species?

ADVANCED
SCIENCE NEWS

www.advancedsciencenews.com

ADVANCED
MATERIALS

www.advmat.de

Table 2. Catalytic performance of recently reported advanced SPFM-mediated electrocatalysts.

Sample ID	React.	Synthesis method	Electrolyte	η [mV]@j [mA cm^{-2}]	Tafel slope [mV dec^{-1}]	Durability	Ref.
Ni–Fe–P–B@CFP	HER	Wet-chemical reduction	1 м KOH	220@10	63	10 mA cm^{-2}, 60 h	[46]
	OER		1 м KOH	269@10	38	100 mA cm^{-2}, 48 h	
						10 mA cm^{-2}, 60 h	
						100 mA cm^{-2}, 48 h	
Li$_x$MoS$_2$	HER	Impregnation and heating	0.1 м H$_2$SO$_4$	165@10	74	23 mA cm^{-2}, 24 h	[66]
NaCo(PO$_3$)$_3$	OER	Solution combustion	1 м KOH	340@10	76	10 mA cm^{-2}, 12 h	[67]
MnGa$_4$/NF	OER	Melting	1 м KOH	291@10	98	10 mA cm^{-2}, 24 h	[68]
BaMoO$_3$	HER	Coprecipitation method	1 м KOH	336@10	110	1000 cycles	[69]
Ni$_x$Fe$_{1-x}$B	HER	Molten salt method	1 м KOH	63.5@10	56.3	10 mA cm^{-2}, 20 h	[70]
	OER		1 м KOH	282@10	86.7	10 mA cm^{-2}, 20 h	
NiO/CeO$_2$ NW@CC	OER	Solvothermal	1 м KOH	330@50	85	50 mA cm^{-2}, 72 h	[71]
SrCo$_{0.85}$Fe$_{0.1}$P$_{0.05}$O$_{3-\delta}$ (SCFP)	OWS	Solid-state reaction	1 м KOH	430@10		10 mA cm^{-2}, 650 h	[90]
Fe$_6$Ge$_5$/NF	OER	High-temperature annealing	1 м KOH	272@100	32	~100 mA cm^{-2}, 25 h	[92]
Ni–Al–Fe–OOH	OER	Atomic layer deposition	0.1 м KOH	346@10	–	CV cycles, 6 h	[105]
Li$_x$NiO/Ni heterostructure	HER	Chemical lithiation	1 м KOH	36@10	50	20 mA cm^{-2}, 50 h	[108]
	HER		1 м Kpi	50@10	66	20 mA cm^{-2}, 50 h	
	HER		0.5 м H$_2$SO$_4$	20@10	31	20 mA cm^{-2}, 50 h	
Li–NiO nanocrystals	OER	Calcination	1 м KOH	289@10	58.1	10 mA cm^{-2}, 70 h	[109]
Na$_{1-x}$Ni$_y$Fe$_{1-y}$O$_2$	OER	Calcination	1 м KOH	260@10	40	10 mA cm^{-2}, 48 h	[112]
Ag-Na$_{0.7}$CoO$_2$	OER	Electrochemical desodiation tuning	1 м KOH	236@10	48	10 mA cm^{-2}, 30 h	[113]
Li$_x$Ni$_{1-x}$O	OER	Solid-state reaction	1 м KOH	370@10	56.6	1000 cycles	[114]
Ni$_{0.9}$Fe$_{0.1}$Co$_{1.975}$Li$_{0.025}$O$_4$	OER	Electrochemical method	1 м KOH	301@10	62	225 mA cm^{-2}, 17 days	[115]
La$_{2-x}$Sr$_x$NiMnO$_6$	OER	Sol–gel and sintering	1 м KOH	490@10	86	1 mA cm^{-2}, 24 h	[116]
NaAl-LRNO	OER	Solid-state reaction	1 м KOH	270@10	69.3	10 mA cm^{-2}, 35 h	[117]
	OER		1 м KOH	331@50	–	10 mA cm^{-2}, 35 h	
	OER		1 м KOH	360@100	–	10 mA cm^{-2}, 35 h	
Na$_2$MnP$_2$O$_7$ polymorphs	OER	Solid-state reaction	0.1 м KOH	450@10	64	500 cycles	[118]
NiFe LDH–Ni(III)Li	OER	Solvothermal	1 м KOH	248@10	35	10 mA cm^{-2}, 24 h	[120]
Na$_{0.67}$CoO$_2$	OER	Solid-state reaction	0.1 м KOH	290@10	39	1000 cycles	[128]
Li–NiMoO$_4$ nanorods	HER	Electrochemical tuning	1 м KOH	73@10	37.2	~70 mA cm^{-2}, 1250 min	[132]
NaFeS$_2$/NF	OER	Hydrothermal	1 м KOH	370@200	94	~28 mA cm^{-2}, 60 h	[136]
GTCo900-KCl/NaCl	HER	Melting	1 м KOH	103@10	70.5	1000 cycles	[137]
			Phosphate buffer	142@10	94.4	1000 cycles	
			0.5 м H$_2$SO$_4$	54@10	52.8	1000 cycles	
Li$^+$ activated WSe$_2$	HER	Hot-injection	0.5 м H$_2$SO$_4$	243@10	116	~ -0.45 V, 12 h	[138]
LiCoBPO/FTO	HER	Hydrothermal	1 м KOH	245@10	58	10 mA cm^{-2}, 25 h	[139]
	OER		1 м KOH	293@10	60	10 mA cm^{-2}, 25 h	
NaCoBPO/FTO	HER	Hydrothermal	1 м KOH	298@10	98	10 mA cm^{-2}, 25 h	[139]
	OER		1 м KOH	328@10	124	10 mA cm^{-2}, 25 h	
LiMnBPO/FTO	OER	Hydrothermal	1 м KOH	≈322@10	41	120 mA cm^{-2}, 1100 h	[140]
NaMnBPO/FTO	OER	Hydrothermal	1 м KOH	≈338@10	47	–	[140]
LiMnBPO/NF	OER	Hydrothermal	1 м KOH	≈228@10	46	20 mA cm^{-2}, 96 h	[140]
NaMnBPO/NF	OER	Hydrothermal	1 м KOH	≈262@10	48	–	[140]
a-LNFBPO	OER	Hydrothermal	1 м KOH	215@10	37	10 mA cm^{-2}, 300 h	[141]

Table 2. Continued.

Sample ID	React.	Synthetis method	Electrolyte	η [mV]@j [mA cm^{-2}]	Tafel slope [mV dec^{-1}]	Durability	Ref.
NdNiO$_3$	OER	Magnetron sputtering	0.1 M KOH	470@0.075	89	–	[143]
Ca-doped Pr$_{0.5}$Ba$_{0.5}$CoO$_{3-\delta}$	OER	Sol–gel and sintering	0.1 M KOH	440@10	73	1000 cycles	[148]
Sr$_2$Fe$_2$O$_{6-\delta}$	OER	Sol–gel and sintering	0.1 M KOH	480@10	60	10 mA cm^{-2}, 500 cycles	[150]
Ba$_{0.5}$Sr$_{0.5}$Co$_{0.8}$Fe$_{0.2}$O$_{3-\delta}$ nanofilms	OER	Sol–gel and sintering	0.1 M KOH	460@10	65	10 000 cycles	[152]
Ba$_{0.5}$Sr$_{0.5}$Co$_{0.8-x}$Fe$_{0.2}$Ni$_x$O$_{3-\delta}$	OER	Sol–gel and sintering	0.1 M KOH	278@10	47.98	10 mA cm^{-2}, 80 h	[155]
SrTi(Ir)O$_3$	OER	Electrospinning and calcination	0.1 M HClO4	265@10	50	10 mA cm^{-2}, 20 h	[156]
h-MoN@BNCNT	HER	Chemical annealing	0.5 M H$_2$SO$_4$	78@10	46	0.05V, 24 h	[157]
Sr$_2$Co$_{1.5}$Fe$_{0.5}$O$_{6-\delta}$	OER	Sol–gel and sintering	1 M KOH	318@10	44.8	1.55 V, 10 h	[159]
Ba(Fe$_{0.7}$Ta$_{0.3}$)O$_{3-\delta}$	HER	Solid-state reaction	0.5 M H$_2$SO$_4$	790@20	117	–	[165]
Mg|Co–MnO$_2$/α-Co(OH)$_2$	OER	Electrochemical method	0.25 M Mg(ClO$_4$)$_2$	–	151	10 mA cm^{-2}, 6 h	[167]
SrRuO$_3$	OER	Liquid-feed flame spray	0.1 M KOH	–	74.2	1.45 V, 24 h	[176]
	OER		0.1 M HClO$_4$	–	51.5	1.45 V, 24 h	
5.0%Ce-NiFe-LDH/CNT	OER	Coprecipitation	1 M KOH	227@10	33	10 mA cm^{-2}, 30 000 s	[178]
Y$_2$Ru$_2$O$_{7-\delta}$	OER	Sol–gel and sintering	0.1 M HClO$_4$	270@2.23	55	1 mA cm^{-2}, 8 h	[180]
Ce$_{0.21}$@Co(OH)$_2$ nanosheets	OER	Microwave treatment	1 M KOH	300@10	72	0.5 V, 12 h	[181]
p-Y$_2$[Ru$_{1.6}$Y$_{0.4}$]O$_{7-\delta}$	OER	Sol–gel and sintering	0.1 M HClO$_4$	270@18.1	37	–	[182]
Ce-doped Ni$_3$S$_2$	OER	Electrodeposition	1 M KOH	257@50	81	0.6 V versus Ag/AgCl, 24 h	[183]
Ce-doped CoP	HER	Hydrothermal and calcination	1 M KOH	92@10	63.5	10 mA cm^{-2}, 10 h	[184]
	HER		0.5 M H$_2$SO$_4$	54@10	54	10 mA cm^{-2}, 10 h	
La(CrMnFeCo$_2$Ni)O$_3$HEPO	OER	Precipitation and calcination	0.1 M KOH	325@10	51.2	10 mA cm^{-2}, 50 h	[185]
Ce-NiBDC/OG nanoarray	OER	Hydrothermal	1 M KOH	265@10	46	1000 cycles	[186]
Co$_3$O$_4$/CeO$_2$ nanohybrids	OER	Electrodeposition	0.5 M H$_2$SO$_4$	423@10	88.1	10 mA cm^{-2}, 50 h	[195]
Co$_3$O$_4$/CeO$_2$ nanohybrids	OER	Solvothermal	1 M KOH	270@10	60	10 mA cm^{-2}, 10 h	[198]
Co$_4$N–CeO$_2$/GP nanosheet	OER	Electrodeposition	1 M KOH	239@10	61	500 mA cm^{-2}, 50 h	[199]
Cu@CeO$_2$@NFC-0.25	OER	Electrodeposition and calcination	1 M KOH	230.8@10	32.7	10 mA cm^{-2}, 30 h	[200]
CeO$_x$/CoS nanoparticles	OER	Solvothermal	1 M KOH	269@10	50	10 mA cm^{-2}, 20 h	[201]
CeO$_x$-coated NiFeO$_x$	OER	Electrodeposition	1 M KOH	–	40	20 mA cm^{-2}, 96 h	[202]
Pd NCs@CeO$_2$	HER	Hydrothermal and calcination	0.5 M H$_2$SO$_4$	–	235	10 000 cycles	[205]
CoSn$_2$/NF	OWS	Solution chemistry	1 M KOH	320@10	–	10 mA cm^{-2}, 16 h	[206]
						100 mA cm^{-2}, 100 h	
FeSn$_2$/NF	OER	One-pot reduction	1 M KOH	197@10	≈31	10 mA cm^{-2}, 24 h	[207]
FeSn$_2$/FTO	OER	One-pot reduction	1 M KOH	273@10	≈33	10 mA cm^{-2}, 24 h	[207]
Co$_2$MnAl	OER	Arc-melting	1 M KOH	–	68	2.5 mA cm^{-2} 12 h	[209]
Co$_2$MnGa	OER	Arc-melting	1 M KOH	–	67	2.5 mA cm^{-2} 12 h	[209]
Al–Ni$_3$S$_2$/NF nanosheet	HER	Solvothermal	1 M KOH	86@10	75	−250 mV, 15 h	[210]
	OER		1 M KOH	223@10	37	1.85 V, 15 h	
Cu$_2$FeSnS$_4$/NF	OER	Mechanical milling	1 M KOH	365@10	37	100 mA cm^{-2}, 24 h	[211]
CoFeBiP nanosheets	OER	Solvothermal	1 M KOH	273@10	77.3	10 mA cm^{-2}, 25 h	[213]
Al, Fe-codoped CoP nanoparticles	HER	Hydrothermal	0.5 M H$_2$SO$_4$	138@10	72	10 mA cm^{-2}, 10 h	[214]
	OER		1 M KOH	280@10	65	10 mA cm^{-2}, 10 h	

Table 2. Continued.

Sample ID	React.	Synthetis method	Electrolyte	η [mV]@j [mA cm^{-2}]	Tafel slope [mV dec^{-1}]	Durability	Ref.
Sn-doped Ni$_5$P$_4$	OER	Hydrothermal and calcination	1 м KOH	173@10	≈46	500 mA cm^{-2}, 12 h	[215]
Ni$_{0.65}$Ga$_{0.30}$Fe$_{0.05}$ nanosheets	OER	Hydrothermal	1 м KOH	200@10	42	20 mA cm^{-2}, 100 h	[216]
Sn$_{0.3}$W$_{0.7}$S$_2$@CB	HER	Hydrothermal	0.5 м H$_2$SO$_4$	–	81	10 mA cm^{-2}, 30 000 s	[218]
Ni$_3$Bi$_2$S$_2$ nanocrystals	HER	Microwave	0.5 м H$_2$SO$_4$	88@10	58	75 mA cm^{-2}, 12 h	[219]
Al–CoS$_2$ nanowires	HER	Melting	0.5 м H$_2$SO$_4$	86@10	62.47	10 mA cm^{-2}, 24 h	[223]
Sn–Ni$_3$S$_2$/NF	HER	Hydrothermal	1 м KOH	170@100	33.8	500 mA cm^{-2}, 70 h	[225]
	OER		1 м KOH	270@100	52.7	500 mA cm^{-2}, 70 h	
Ni$_{1.5}$Sn@triMPO$_4$-R	OER	Precipitation and calcination	1 м KOH	240@10	45.2	1.56 V, 10 h	[227]
Al$_{80}$Ni$_6$Co$_3$Mn$_3$Y$_5$Au$_3$	HER	Arc melting	0.5 м H$_2$SO$_4$	70@10	39	10 mA cm^{-2}, 20 h	[229]
Mn/Co/Zn-codoped MSN-Cs nanoclusters	HER	Wet chemistry synthesis	1 м KOH	176@10	43	10 mA cm^{-2}, 50 000 cycles	[230]
Ca-doped CuCoO$_2$ nanosheets	OER	Hydrothermal	1 м KOH	470@10	96.5	10 mA cm^{-2}, 18 h	[231]
FeAs intermetallic	OER	Hot-injection	1 м KOH	330@100	≈32	10 mA cm^{-2}, 24 h	[234]
FeSi/NF	OER	High-temperature solid-state method	1 м KOH	220@10	39	10 mA cm^{-2}, 24 h	[236]
NiGe/NF	OER	Hot-injection	1 м KOH	228@10	≈56	1.48 V, 505 h	[237]
NiGe/FTO	OER	Hot-injection	1 м KOH	322@10	–	1.58 V, 24 h	
Si-SCO	OER	Ball-milling-assisted solid-state reaction	0.1 м KOH	417@10	66	–	[238]
Co$_{2.4}$Ni$_{0.6}$Ge$_2$O$_5$(OH)$_4$ nanosheets	OER	Hydrothermal method	1 м KOH	255@10	59.8	10 mA cm^{-2}, 20 h	[239]
Sr$_2$Fe$_{0.67}$Co$_{0.67}$Ge$_{1.66}$O$_7$	OER	Sol–gel and sintering	4 м KOH	–	39	10 mA cm^{-2}, 12 h	[240]
Ni–Fe–Sn	HER	One-step potentiostatic electrodeposition route	1 м KOH	180@100	149	10 mA cm^{-2}, 12 h	[248]
V$_O$B–Co$_3$O$_4$/NF nanowire	HER	Hydrothermal-calcination-reduction	1 м KOH	184@50	60.7	10 mA cm^{-2}, 20 h	[252]
	OER		1 м KOH	315@50	112.5	10 mA cm^{-2}, 20 h	
B-Co$_2$Fe LDH	OER	Water bath and redution	1 м KOH	205@10	39.2	100 mA cm^{-2}, 100 h	[253]
N,Ru codoped Sb$_2$S$_3$	HER	Reflux method	1 м KOH	72@10	193	10 mA cm^{-2}, 10 h	[255]
Trirutile CoSb$_2$O$_6$	OER	Sol–gel and sintering	1 м KOH	360@100	46	100 mA cm^{-2}, 120 h	[256]
Ni–W–B/CC	HER	Electroless plating	1 м KOH	101@100	119.1	100 mA cm^{-2}, 20 h	[260]
	OER		1 м KOH	344@100	130.1	100 mA cm^{-2}, 20 h	

Note: OWS denotes the overall water splitting.

ii) can such chemical stability enhanced by the SPFM species be extended to various electrolytes under different conditions (concentration, temperature, Fe impurity, and pH value)? Note that under cathodic HER, according to the Pourbaix diagram, the leaching of prime active NNTM,[266] i.e., Ni, Co, Fe, and Cu, can also occur, the related investigation on whether and how SPFM species protect the HER-active NNTM catalysts from corrosion is still ambiguous. On the other hand, there is currently a common cognition that the structural reconstruction of NNTM-based precatalysts to the corresponding TM-based (oxy)hydroxides is almost inevitable during OER. It should be noted that a higher transformation degree usually ensures a better activity.[97] To this end, one main aim of introducing the SPFM species is to accelerate the phase transformation during OER. Moreover, to the best of our knowledge, considerable SPFM-mediated NNTM-based electrocatalysts exhibited a high capability to retain their original structure during the HER process.[105,206,218,267] This might be due to the partial electrons transfer toward NNTM from SPFM species, by increasing the charge density at the d-band orbitals of NNTM, and accordingly, preventing the severe (hydro)oxidation of TM, thereby optimizing their stability.[44,96] On the whole, although

**ADVANCED
SCIENCE NEWS**

www.advancedsciencenews.com

**ADVANCED
MATERIALS**

www.advmat.de

the operation stability of the NNTM-based electrocatalysts could be remarkably enhanced in the presence of SPFM species, the detailed analysis of the stabilizing mechanism is still currently unclear. In addition to this, the synthetic methods for such SPFM-mediated electrocatalysts have also been provided in Table 2. Obviously, various kinds of synthetic methods such as melting, solvothermal, electrochemical intercalation, and hot-injection approaches are viable for these electrocatalysts, signifying that these electrocatalysts can be obtained through various strategies.

3.6. Horizontal Discussion of the SPFM Species

As discussed above, although s-, p-, and f-block metals toward water splitting exhibit inert or low activity, they have shown a competitive edge in mediating the NNTM-based electrocatalysts. Their competitive edge mainly contains the following aspects. i) Most of these s-, p-, and f-block metals are earth-abundant and low cost, and many synthetic approaches such as melting, solvothermal, electrochemical intercalation, hot-injection, and template methods could be employed to incorporate these metal species into NNTM-based compounds. ii) s-, p-, and f-block metal species provide more possibilities to boost the intrinsic catalytic activity of NNTM-based electrocatalysts because they can realize the hybridization of the d-orbital electron of NNTM atoms with s-, p-, and f-orbital electron of SPFM atoms. iii) Most of these SPFM hold the metallic feature, showing higher conductivity as compared to many anions, and also most of them could bind NNTM to generate a variety of novel intermetallics, offering the platform to develop advanced electrocatalysts for water splitting. iv) Many SPFM species present unique physical and chemical features, such as the intercalation of alkali metals and the photothermal effect. Since the research on the SPFM-mediated NNTM-based electrocatalysts for water splitting is in its infancy, we believe there are still many interesting, unknown, and unique advantages of SPFM conducing to the improvement of the activity that deserves future attention. Moreover, it could also be concluded from the above parts that although the SPFM species exhibited many similar roles in mediating the catalytic activity of NNTM-based electrocatalysts, these metal species also showed different catalytic behavior to some extent. To better reflect that the main stated point is based on the periodic table, the Pourbaix diagrams for the representative SPFM species such as Li, Ba, Ce, Sn, and As in the water system are first provided in Figures S1–S5 of the Supporting Information. Pourbaix diagram, which is one kind of thermodynamic equilibrium diagram (E vs pH), is constructed based on the analysis of the possible chemical and electrochemical equilibria in the system. It can be achieved by the theoretical calculation method. For comparison, the Pourbaix diagram for Fe, which is a typical metal species from d-block metal was also provided in Figure S6 of the Supporting Information.[268] As seen in the Pourbaix diagram for the Fe-water system, Fe species tend to form their corresponding hydroxide during the alkaline OER and HER process. However, the chemical corrosion occurred for Fe during the acidic OER and HER process albeit the metallic state can be maintained to a large extent during HER. Compared to this, alkali metal

Li species is prone to be converted to the Li$^+$ during both OER and HER through the whole pH range.[269] As for the Ba-water system, BaOH$^+$ can be formed during OER in alkaline media; while Ba^{2+} is the dominated species during OER in acidic media and HER in alkaline and acidic media.[270] Theoretically, copresence of metal hydroxide and oxide for rare earth metal Ce can be observed during OER in alkaline media while only the metal hydroxide was formed during the acidic media.[268] For HER, in the alkaline and acidic media, the metal hydroxide and Ce^{3+} are generated, respectively. The lean metal Sn species would transform to be the Sn^{3+} and HSnO$_2^+$ during OER and HER in alkaline media, respectively; while they form Sn^{2+}/SnO$_2$ and Sn^{2+}/SnOH$^+$/Sn during OER and HER in acidic media, respectively.[266] With the metalloid As species, AsO$_4^{3-}$ and H$_3$AsO$_4$ are formed preferentially during OER in alkaline and acidic media, respectively; while AsO$_2$OH^{2-} and As(OH)$_3$ is formed during HER in alkaline and acidic media, respectively.[271] Apparently, it can be concluded that different types of metal species exhibit distinct transformation behavior during water splitting, which is probably one main cause for the different catalytic mechanisms.

Apart from the distinct transformation behavior during water splitting, the different electronic configuration and atomic radius also contributed to the dissimilar merits and demerits of s-, p-, and f-block metals for water splitting to some extent. i) In s-block metals where alkali metal and alkaline earth metal species are included, the former one bear quite high reactivity and small atomic radius, which competently enable them to be intercalated into the layer of NNTM-based compounds (e.g., metal (oxy)hydroxides) and thereby optimizing of the catalytic activity by expanding the layer distance and altering the electronic structure. Unfortunately, it seems hard for them to bind with NNTM to form some novel and stable intermetallics due to their mismatched atomic radius and the strong reduction ability of alkali metals, limiting the diversity of catalytic systems. ii) Compared to alkali metals, the intercalation of alkaline-earth metals into metal (oxy)hydroxides have been confirmed to suppress the activity due to their strong affinity toward O atoms from electrolytes, which disturbs the interlayer network of water molecules and effectively inhibits the interaction with surface intermediates. Note that the intermetallics based on alkaline-earth metal can be formed, but their relevant application in the field of water splitting is still at the nascent stage, which may be a deserved topic for future investigations. The current popular reported merit for the alkaline-earth metal is employing them as one important chemical species to construct the perovskites-based electrocatalysts for water splitting. iii) In comparison to s-block metals, f-block metals mainly refer to the rare earth metal species. Because of the large atomic radius, these rare earth metals are almost impossible to intercalate into the layer of NNTM-based compounds. Meanwhile, the large relative atomic mass of rare earth metal elements usually decreases the mass-normalized activity. Despite these demerits, rare earth metal-based oxides are quite stable during catalysis and can serve as a confinement matrix for the active NNTM-based compounds, which can inhibit the aggregation and dissolution of the NNTM-based phase to a large extent, thus attaining a high activity. Moreover, numerous rare earth metal-based intermetallics could be formed with suitable elements, which

ADVANCED
SCIENCE NEWS
www.advancedsciencenews.com

**ADVANCED
MATERIALS**
www.advmat.de

are expected to exhibit superior catalytic activity. iv) p-block metal species contain lean metals and metalloids. Among them, the prominent advantage of lean metals is employing them to bind with NNTM to form the intermetallics which can deliver exceptional catalytic performance. Remarkably, during catalysis, the surface of intermetallics is reconstructed while the core with high intrinsic conductivity is well maintained, resulting in synergistic catalysis. Moreover, the surficial lean metals are usually dissolved in the electrolyte, contributing to the generation of porous active nanodomains. However, when they are implemented toward practical application, the economical recycling of the dissolved lean metals in an environmental way may be a challenge. Moreover, the intercalation of lean metal species into the layer of NNTM-based (oxy)hydroxide has scarcely been reported. v) Similar to lean metals, metalloids can also be utilized to bind with NNTM to form intermetallics. Furthermore, superior to the lean metals, it was discovered that some metalloids (e.g., B and Si) with small atomic radius could be inserted into the layer of NNTM-based (oxy)hydroxide. The unique merit for the metalloids is also to dope them (such as B) into NNTM-based compounds not only modify the electronic structure and lattice strain but also trigger the photothermal effect, which is beneficial for the improvement of the activity. However, the conductivity of B and Si may also be an issue to the catalytic system. Moreover, As and Sb are harmful to the surroundings and therefore, special attention is required to recycle them economically and environmentally.

Since the electronic structure directly determines the conductivity and adsorption free energy of the intermediates, establishing the composition–electronic structure–activity correlation is of great significance.[272] The electronic structure intrinsically refers to the spin ordering, energy band structure (e.g., d-band), and density of state.[273] Generally, strategies such as doping, intercalation, heterojunction, and construction of unique phase structures can effectively trigger the generation of vacancy, strain, and/or phase transition, thus adjusting the electronic structure.[272,273] As discussed in Sections 3.1–3.5, nearly the above-outlined strategies could be adopted to all SPFM species to tune the electronic structure. Herein, based on the discussion in the last paragraph, the preferable and typical tuning of the electronic structure to NNTM-based electrocatalysts by each type of SPFM species is provided in the following. i) The intercalation of alkali metal species into layered NNTM-based electrocatalysts could cause the charge polarization and strengthen the hybridization between the NNTM and anion species.[114] It could also induce the polymorphic phase transition and then optimize the electronic structure, increasing the catalytic activity. For example, when Li was intercalated into the pristine MoS_2, the phase transition from the 2H-type MoS_2 to the 1T-type Li_xMoS_2 occurred by injecting extra charges accumulated in the MoS_2 layers and enhanced the d-band filling level of the Mo atom. In the meantime, the oxidation state of the Mo species was decreased.[274] These variations in the electronic structure effectively reduced the reaction barriers for catalysis. ii) In the alkaline-earth metal-based perovskites, oxygen vacancies are always generated, leading to a geometrical effect and orbital hybridization, and thus an activity enhancement.[275] Taking $Ca_2Mn_2O_5$ OER electrocatalyst as an example, the Mn^{3+} with $t_{2g}^3 e_g^1$ configuration in the structure

readily adsorb the OH^- provided a high spin state is available to overlap the O-p_σ orbit of OH^- ions and activated the oxygen vacancies near to the Mn^{3+} as the adsorption site.[161] Furthermore, the high degree of overlapped orbitals expedited the ion exchange and decreased the energy barrier for the rate-determining step.[276] iii) The coupling of rare earth metal oxide with the NNTM-based phase to build the heterostructure could not only contribute to the formation of oxygen vacancies around the interface but also gave rise to the charge interaction between these two phases.[71] On the one hand, the defect accompanied with the charge interaction facilitated the transformation of the NNTM-based phase to corresponding NNTM-based (oxy)hydroxide active phases during OER. On the other hand, the stable rare earth metal oxide could further electronically interplay with the active phase, optimizing the Gibbs adsorption free energy toward intermediates. Typically, oxygen vacancies around the interface of the CeO_2/NiO heterostructure were beneficial for the transformation of NiO to NiOOH active phase. Furthermore, the charge injection of CeO_2 into the transformed NiOOH decreased the adsorption free energy barrier of the rate-determining step from the conversion of *–O to *–OOH.[71] iv) Binding the lean metals with the NNTM to form intermetallics could effectively maintain the high conductivity owing to the orbital hybridization between two metal species, which assures a certain number of electrons located around the Fermi level.[96] Such a high conductivity promotes the charge transfer during catalysis by accelerating the surface transformation to the NNTM-based (oxy)hydroxide active phase, as confirmed by the catalytic behavior of $FeSn_2$ and $MnGa_4$.[68,207] v) Doping of metalloids into NNTM-based compounds (e.g., oxides) capture electrons from NNTM and transfer them to neighboring anion atoms owing to their moderate electronegativity.[277] Electron-enriched or -depleted local regions can favorably be generated on the surface which may be beneficial for maximizing the number of active sites for electrocatalytic water splitting. Similarly, electronic coupling interactions between metal d-orbitals and metalloid sp-orbitals can shift the center of the d-orbital from the Fermi level, optimizing the free adsorption energy and reaction kinetics toward the intermediates.[228]

Therefore, based on the above comparison, the following modification strategy may be considered when one wants to utilize the SPFM to mediate the NNTM-based electrocatalysts. That is, i) the alkali metals probably be suitably used for intercalation, ii) the alkaline-earth metals are the promising component to construct the perovskites with unique structure, iii) the rare earth metals can be competently created as a confinement subunit, iv) the lean metals can be rationally employed to bind with NNTM to form the intermetallics, and v) the metalloids can be preferentially exploited for doping. Moreover, synergistic catalysis is highly expected to be achieved by incorporating the above two or more SPFM species.

4. Open Research Questions

In this review, we discussed the recent efforts toward the development of SPFM-containing transition metal-based electrocatalysts for efficient HER, OER, and overall water splitting. Most of such electrocatalytic systems exhibit superior HER

and OER activity, which can be explained by means of composition–structure–dynamic–activity relationships and the particular role of the nontransition metal in the system. This knowledge is expected to pave the way to more efficient SPFM-tuned electrocatalysts with optimized catalytic activity. Up to now, the topic of SPFM-containing electrocatalysts to boost water splitting is still in its infancy. Far more theoretical modeling toward the identification of descriptors is needed to shed new light on the pivotal role of SPFM atoms to bring about a predictive design of such materials. Major experimental and technical challenges and opportunities embrace the following research questions.

i) Besides SPFM-containing transition metal catalysts, which show promising performance in electrocatalytic water splitting, can one generate and use a solely SPFM atom-based (e.g., Ge) electrocatalyst for both HER and OER, where a single s-, p-, and f-block metal acts as an active site? As recent investigations in this direction have demonstrated that sole alkaline-earth metal electrocatalysts can be efficiently utilized for reduction reactions, more efforts should be devoted to explore new SPFM-based catalytic systems without the involvement of transition metals for water splitting.

ii) Could one enhance the performance of SPFM-containing electrocatalysts for efficient HER and OER through integrating them with advanced compounds such as intermetallics and f-block metal-containing perovskites (heterostructuring)? By doing this, more SPFM-mediated transition metal electrocatalysts could be innovatively developed that can synergistically bear the optimized catalytic activity toward HER and OER.

iii) How to realize a highly active SPFM-containing system that endures under the currently harsh technical conditions (high temperature, high pressure, high-concentrated alkaline or acidic media, large current density) during water splitting? Understanding the catalytic behavior of SPFM-containing systems under harsh conditions is of great significance to propel their practical application of future water electrolysis.

iv) Can the SPFM-containing system with high efficiency be developed for seawater splitting? Since seawater is one of the most abundant natural resources on our planet (more than 96% of total water resources on the earth), enabling direct electrolysis of seawater will greatly reduce the dependence on pure water.

v) Can the leaching or redeposition of those s-, p-, and f-block elements during electrocatalysis be visually reflected by the in situ TEM measurement? And accordingly, whether the local structure and valence variation of those elements during electrocatalysis can be probed by the operando XAS? By these means, the catalytic mechanism of these metals can be clarified at the atomic level, which provides a theoretical basis and evidence for the further design of high-performance electrocatalysts.

vi) Besides kinetics and thermodynamics simulation, is it theoretically possible to calculate and predict optimal materials containing s-, p-, and f-block metals to endure long-term stability? Since the long-term stability of electrocatalyst, especially at large current densities, is an unsolved issue

and a prerequisite for practical application, the theoretical models conducted in advance will be highly meaningful.

vii) Can one develop a facile approach to synthesize bifunctional SPFM-mediated transition metal-based electrocatalysts with low-cost, high activity, increased surface area on a large scale (kg-level)? Developing an abundant and scalable synthesis of SPFM-based materials has been a major barrier so far which plays a vital role in the large-scale industrial application of bifunctional electrocatalysts.

viii) Apart from the metals discussed above, can one comprehensively explore the effects of other p- and f-block metals (such as halogens or other lanthanide series of metals) on water electrolysis? How will they influence the structural and electronic properties of the transition metals? This information can be implemented in machine learning to make a fast prediction, to build better models, and to generate new knowledge on design blueprints for enhanced catalytic activity.

ix) Could one systematically modify and implement the SPFM-containing electrocatalysts in other important electrocatalytic reactions such as the $2e^-$-dominated oxygen reduction reaction and CO_2 reduction? The purpose of the oxygen reduction reaction could be to enable a facile formation of hydrogen peroxide (H_2O_2), which is a benign chemical oxidant with a variety of applications in industrial processes such as paper bleaching, water treatment, and chemical synthesis. Once these SPFM-containing electrocatalysts are found to be effective for such desired electrocatalytic applications, they will likely trigger more attention in terms of their structural optimization to achieve maximized energetic efficiencies.

Supporting Information

Supporting Information is available from the Wiley Online Library or from the author.

Acknowledgements

Conflict of Interest

The authors declare no conflict of interest.

**ADVANCED
SCIENCE NEWS**

www.advancedsciencenews.com

**ADVANCED
MATERIALS**

www.advmat.de

Keywords

catalytic mechanism, precatalysts, s-, p-, and f-block, transition metals, water splitting

[1] S. Carley, D. M. Konisky, *Nat. Energy* **2020**, *5*, 569.

[2] B. Joshi, E. Samuel, Y. L. Kim, A. L. Yarin, M. T. Swihart, S. S. Yoon, *Adv. Funct. Mater.* **2021**, *31*, 2008181.

[3] Z. P. Ifkovits, J. M. Evans, M. C. Meier, K. M. Papadantonakis, N. S. Lewis, *Energy Environ. Sci.* **2021**, *14*, 4740.

[4] H. Y. Yang, P. W. Menezes, M. Driess, *Adv. Energy Mater.* **2021**, *11*, 2102074.

[5] S. Anantharaj, S. Noda, V. R. Jothi, S. C. Yi, M. Driess, P. W. Menezes, *Angew. Chem., Int. Ed.* **2021**, *60*, 18981.

[6] C. Panda, P. W. Menezes, M. Driess, *Angew. Chem., Int. Ed.* **2018**, *57*, 11130.

[7] Y. Li, Y. Sun, Y. Qin, W. Zhang, L. Wang, M. Luo, H. Yang, S. Guo, *Adv. Energy Mater.* **2020**, *10*, 1903120.

[8] L. Tian, Z. Li, M. Song, J. Li, *Nanoscale* **2021**, *13*, 12088.

[9] Q. Shi, C. Zhu, D. Du, Y. Lin, *Chem. Soc. Rev.* **2019**, *48*, 3181.

[10] A. Chalgin, C. Song, P. Tao, W. Shang, T. Deng, J. Wu, *Prog. Nat. Sci.* **2020**, *30*, 289.

[11] J. Ying, G. Jiang, Z. P. Cano, L. Han, X. Y. Yang, Z. Chen, *Nano Energy* **2017**, *40*, 88.

[12] S. Ye, F. Luo, T. Xu, P. Zhang, H. Shi, S. Qin, J. Wu, C. He, X. Ouyang, Q. Zhang, J. Liu, X. Sun, *Nano Energy* **2020**, *68*, 104301.

[13] F. Y. Yu, Z. L. Lang, L. Y. Yin, K. Feng, Y. J. Xia, H. Q. Tan, H. T. Zhu, J. Zhong, Z. H. Kang, Y. G. Li, *Nat. Commun.* **2020**, *11*, 490.

[14] J. Y. Chen, P. X. Cui, G. Q. Zhao, K. Rui, M. M. Lao, Y. P. Chen, X. S. Zheng, Y. Z. Jiang, H. G. Pan, S. X. Dou, W. P. Sun, *Angew. Chem., Int. Ed.* **2019**, *58*, 12540.

[15] Y. Hu, G. Luo, L. Wang, X. Liu, Y. Qu, Y. Zhou, F. Zhou, Z. Li, Y. Li, T. Yao, C. Xiong, B. Yang, Z. Yu, Y. Wu, *Adv. Energy Mater.* **2021**, *11*, 2002816.

[16] B. S. Yeo, *Nat. Catal.* **2019**, *2*, 284.

[17] P. Su, W. Pei, X. Wang, Y. Ma, Q. Jiang, J. Liang, S. Zhou, J. Zhao, J. Liu, G. Q. Lu, *Angew. Chem., Int. Ed.* **2021**, *60*, 16044.

[18] W. H. Lee, Y. J. Ko, J. Y. Kim, B. K. Min, Y. J. Hwang, H. S. Oh, *Chem. Commun.* **2020**, *56*, 12687.

[19] C. Cui, R. F. Cheng, H. Zhang, C. Zhang, Y. H. Ma, C. Shi, B. B. Fan, H. L. Wang, X. H. Wang, *Adv. Funct. Mater.* **2020**, *30*, 2000693.

[20] Y. Wu, X. Li, Y. Wei, Z. Fu, W. Wei, X. Wu, Q. Zhu, Q. Xu, *Adv. Mater.* **2021**, *33*, 2006965.

[21] X. Han, X. Wu, Y. Deng, J. Liu, J. Lu, C. Zhong, W. Hu, *Adv. Energy Mater.* **2018**, *8*, 1800935.

[22] X. J. Cui, P. J. Ren, C. Ma, J. Zhao, R. X. Chen, S. M. Chen, N. P. Rajan, H. B. Li, L. Yu, Z. Q. Tian, D. H. Deng, *Adv. Mater.* **2020**, *32*, 1908126.

[23] M. Zhou, S. Bao, A. J. Bard, *J. Am. Chem. Soc.* **2019**, *141*, 7327.

[24] Y. Peng, B. Lu, S. Chen, *Adv. Mater.* **2018**, *30*, 1801995.

[25] W. H. Lai, L. F. Zhang, W. B. Hua, S. Indris, Z. C. Yan, Z. Hu, B. Zhang, Y. Liu, L. Wang, M. Liu, R. Liu, Y. X. Wang, J. Z. Wang, Z. Hu, H. K. Liu, S. L. Chou, S. X. Dou, *Angew. Chem., Int. Ed.* **2019**, *58*, 11868.

[26] Y. Yang, Y. Yang, Z. Pei, K.-H. Wu, C. Tan, H. Wang, L. Wei, A. Mahmood, C. Yan, J. Dong, S. Zhao, Y. Chen, *Matter* **2020**, *3*, 1442.

[27] S. Ye, F. Luo, Q. Zhang, P. Zhang, T. Xu, Q. Wang, D. He, L. Guo, Y. Zhang, C. He, X. Ouyang, Q. Wang, M. Gu, J. Liu, X. Sun, *Energy Environ. Sci.* **2019**, *12*, 1000.

[28] X. Hu, G. Luo, Q. Zhao, D. Wu, T. Yang, J. Wen, R. Wang, C. Xu, N. Hu, *J. Am. Chem. Soc.* **2020**, *142*, 16776.

[29] J. Shan, T. Ling, K. Davey, Y. Zheng, S. Z. Qiao, *Adv. Mater.* **2019**, *31*, 1900510.

[30] J. Wang, Y. Ji, R. Yin, Y. Li, Q. Shao, X. Huang, *J. Mater. Chem. A* **2019**, *7*, 6411.

[31] H. Wang, Y. Yang, F. J. DiSalvo, H. D. Abruña, *ACS Catal.* **2020**, *10*, 4608.

[32] W. Xiao, W. Lei, M. Gong, H. L. Xin, D. Wang, *ACS Catal.* **2018**, *8*, 3237.

[33] M. Varshney, A. Sharma, H. J. Shin, H. H. Lee, T. Y. Jeon, B. H. Lee, K. H. Chae, S. O. Won, *J. Phys. Chem. Solids* **2017**, *110*, 187.

[34] L. W. Chen, X. Guo, R. Y. Shao, Q. Q. Yan, L. L. Zhang, Q. X. Li, H. W. Liang, *Nano Energy* **2021**, *81*, 105636.

[35] C. Panda, P. W. Menezes, M. Zheng, S. Orthmann, M. Driess, *ACS Energy Lett.* **2019**, *4*, 747.

[36] Z. Chen, H. Qing, K. Zhou, D. Sun, R. Wu, *Prog. Mater Sci.* **2020**, *108*, 100618.

[37] C. Walter, P. W. Menezes, S. Orthmann, J. Schuch, P. Connor, B. Kaiser, M. Lerch, M. Driess, *Angew. Chem., Int. Ed.* **2017**, *57*, 698.

[38] B. Chakraborty, S. Kalra, R. Beltrán-Suito, C. Das, T. Hellmann, P. W. Menezes, *Chem. Asian. J.* **2020**, *15*, 852.

[39] S. Yao, V. Forstner, P. W. Menezes, C. Panda, S. Mebs, E. M. Zolnhofer, M. E. Miehlich, T. Szilvási, N. A. Kumar, M. Haumann, K. Meyer, H. Grutzmacher, M. Driess, *Chem. Sci.* **2018**, *9*, 8590.

[40] R. Beltrán-Suito, P. W. Menezes, M. Driess, *J. Mater. Chem. A* **2019**, *7*, 15749.

[41] Z. Y. Yu, Y. Duan, X. Y. Feng, X. X. Yu, M. R. Gao, S. H. Yu, *Adv. Mater.* **2021**, *33*, 2007100.

[42] F. Yu, L. Yu, I. K. Mishra, Y. Yu, Z. F. Ren, H. Q. Zhou, *Mater. Today Phys.* **2018**, *7*, 121.

[43] S. Sultan, J. N. Tiwari, A. N. Singh, S. Zhumagali, M. Ha, C. W. Myung, P. Thangavel, K. S. Kim, *Adv. Energy Mater.* **2019**, *9*, 1900624.

[44] S. Gupta, M. K. Patel, A. Miotello, N. Patel, *Adv. Funct. Mater.* **2020**, *30*, 1906481.

[45] K. Y. Yoon, J. Park, M. Jung, S. G. Ji, H. Lee, J. Seo, M. J. Kwak, S. I. Seok, J. H. Lee, J. H. Jang, *Nat. Commun.* **2021**, *12*, 4309.

[46] W. Tang, X. Liu, Y. Li, Y. Pu, Y. Lu, Z. Song, Q. Wang, R. Yu, J. Shui, *Nano Res.* **2020**, *13*, 447.

[47] J. Fournier, P. K. Wrona, A. Lasia, R. Lacasse, J. M. Lalancette, H. Menard, L. Brossard, *J. Electrochem. Soc.* **1992**, *139*, 2372.

[48] N. M. Marković, S. T. Sarraf, H. A. Gasteiger, P. N. Ross, *J. Chem. Soc., Faraday Trans.* **1996**, *92*, 3719.

[49] R. Otogawa, M. Morimitsu, M. Matsunaga, *Electrochim. Acta* **1998**, *44*, 1509.

[50] T. Ioroi, N. Kitazawa, K. Yasuda, Y. Yamamoto, H. Takenaka, *J. Appl. Electrochem.* **2001**, *31*, 1179.

[51] T. Lister, Y. Tolmachev, Y. Chu, W. Cullen, H. You, R. Yonco, Z. Nagy, *J. Electroanal. Chem.* **2003**, *554*, 71.

[52] V. Stamenković, M. Arenz, P. Ross, N. Marković, *J. Phys. Chem. B* **2004**, *108*, 17915.

[53] Y. Y. Hou, J. M. Hu, L. Liu, J. Q. Zhang, C. N. Cao, *Electrochim. Acta* **2006**, *51*, 6258.

[54] J. Jirkovský, M. Makarova, P. Krtil, *Electrochem. Commun.* **2006**, *8*, 1417.

[55] M. P. M. Kaninski, V. M. Nikolić, T. N. Potkonjak, B. R. Simonović, N. I. Potkonjak, *Appl. Catal., A* **2007**, *321*, 93.

[56] K. Macounová, J. Jirkovský, M. V. Makarova, J. Franc, P. Krtil, *J. Solid State Electrochem.* **2009**, *13*, 959.

**ADVANCED
SCIENCE NEWS**

www.advancedsciencenews.com

**ADVANCED
MATERIALS**

www.advmat.de

[57] V. Petrykin, K. Macounova, O. Shlyakhtin, P. Krtil, *Angew. Chem., Int. Ed.* **2010**, *49*, 4813.

[58] Y. Li, P. Hasin, Y. Wu, *Adv. Mater.* **2010**, *22*, 1926.

[59] R. Subbaraman, D. Tripkovic, K. C. Chang, D. Strmcnik, A. P. Paulikas, P. Hirunsit, M. Chan, J. Greeley, V. Stamenkovic, N. M. Markovic, *Nat. Mater.* **2012**, *11*, 550.

[60] W. F. Chen, S. Iyer, S. Iyer, K. Sasaki, C. H. Wang, Y. Zhu, J. T. Muckerman, E. Fujita, *Energy Environ. Sci.* **2013**, *6*, 1818.

[61] J. Ren, M. Antonietti, T. P. Fellinger, *Adv. Energy Mater.* **2014**, *5*, 1401660.

[62] J. Kibsgaard, C. Tsai, K. Chan, J. D. Benck, J. K. Nørskov, F. Abild-Pedersen, T. F. Jaramillo, *Energy Environ. Sci.* **2015**, *8*, 3022.

[63] P. Cai, J. Huang, J. Chen, Z. Wen, *Angew. Chem., Int. Ed.* **2017**, *56*, 4858.

[64] S. Keltie, *J. Mater. Chem. A* **2018**, *6*, 24988.

[65] L. Zhang, Y. Jia, G. Gao, X. Yan, N. Chen, J. Chen, M. T. Soo, B. Wood, D. Yang, A. Du, X. Yao, *Chem* **2018**, *4*, 285.

[66] L. Wu, N. Y. Dzade, M. Yu, B. Mezari, A. J. van Hoof, H. Friedrich, N. H. de Leeuw, E. J. Hensen, J. P. Hofmann, *ACS Energy Lett.* **2019**, *4*, 1733.

[67] R. Gond, D. K. Singh, M. Eswaramoorthy, P. Barpanda, *Angew. Chem., Int. Ed.* **2019**, *58*, 8330.

[68] P. W. Menezes, C. Walter, J. N. Hausmann, R. Beltrán-Suito, C. Schlesiger, S. Praetz, V. Y. Verchenko, A. V. Shevelkov, M. Driess, *Angew. Chem., Int. Ed.* **2019**, *58*, 16569.

[69] X. Xu, Y. Pan, Y. Zhong, L. Ge, S. Jiang, Z. Shao, *Composites, Part B* **2020**, *198*, 108214.

[70] W. Hong, S. Sun, Y. Kong, Y. Hu, G. Chen, *J. Mater. Chem. A* **2020**, *8*, 7360.

[71] H. Yang, G. Dai, Z. Chen, J. Wu, H. Huang, Y. Liu, M. Shao, Z. Kang, *Small* **2021**, *17*, 2101727.

[72] L. Yang, Z. Liu, S. Zhu, L. Feng, W. Xing, *Mater. Today Phys.* **2021**, *16*, 100292.

[73] H. J. Liu, B. Dong, *Mater. Today Phys.* **2020**, *20*, 100469.

[74] L. B. Wu, L. Yu, X. Xiao, F. H. Zhang, S. W. Song, S. Chen, Z. F. Ren, *Research* **2020**, *2020*, 3976278.

[75] P. J. McHugh, A. D. Stergiou, M. D. Symes, *Adv. Energy Mater.* **2020**, *10*, 2002453.

[76] C. Hu, L. Zhang, J. Gong, *Energy Environ. Sci.* **2019**, *12*, 2620.

[77] H. J. Song, H. Yoon, B. Ju, D. W. Kim, *Adv. Energy Mater.* **2020**, *11*, 2002428.

[78] H. Zhang, A. W. Maijenburg, X. P. Li, S. L. Schweizer, R. B. Wehrspohn, *Adv. Funct. Mater.* **2020**, *30*, 2003261.

[79] M.-I. Jamesh, M. Harb, *J. Energy Chem.* **2021**, *56*, 299.

[80] L. K. Gao, X. Cui, C. D. Sewell, J. Li, Z. Q. Lin, *Chem. Soc. Rev.* **2021**, *50*, 8428.

[81] C. Niether, S. Faure, A. Bordet, J. Deseure, M. Chatenet, J. Carrey, B. Chaudret, A. Rouet, *Nat. Energy* **2018**, *3*, 476.

[82] L. K. Gao, X. Cui, Z. W. Wang, C. D. Sewell, Z. L. Li, S. Liang, M. Y. Zhang, J. Li, Y. J. Hu, Z. Q. Lin, *Proc. Natl. Acad. Sci. USA* **2021**, *118*, e2023421118.

[83] J. Song, C. Wei, Z. F. Huang, C. Liu, L. Zeng, X. Wang, Z. J. Xu, *Chem. Soc. Rev.* **2020**, *49*, 2196.

[84] X. F. Lu, Y. Fang, D. Luan, X. W. D. Lou, *Nano Lett.* **2021**, *21*, 1555.

[85] S. Anantharaj, S. Noda, M. Driess, P. W. Menezes, *ACS Energy Lett.* **2021**, *6*, 1607.

[86] C. Panda, P. W. Menezes, S. Yao, J. Schmidt, C. Walter, J. N. Hausmann, M. Driess, *J. Am. Chem. Soc.* **2019**, *141*, 13306.

[87] B. Chakraborty, R. Beltrán-Suito, V. Hlukhyy, J. Schmidt, P. W. Menezes, M. Driess, *ChemSusChem* **2020**, *13*, 3222.

[88] C. Panda, P. W. Menezes, C. Walter, S. Yao, M. E. Miehlich, V. Gutkin, K. Meyer, M. Driess, *Angew. Chem., Int. Ed.* **2017**, *129*, 10642.

[89] P. W. Menezes, A. Indra, C. Das, C. Walter, C. Göbel, V. Gutkin, D. Schmeißer, M. Driess, *ACS Catal.* **2017**, *7*, 103.

[90] G. Chen, Z. Hu, Y. Zhu, B. Gu, Y. Zhong, H. J. Lin, C. T. Chen, W. Zhou, Z. Shao, *Adv. Mater.* **2018**, *30*, 1804333.

[91] P. W. Menezes, C. Panda, S. Loos, F. Bunschei-Bruns, C. Walter, M. Schwarze, X. Deng, H. Dau, M. Driess, *Energy Environ. Sci.* **2018**, *11*, 1287.

[92] J. N. Hausmann, R. A. Khalaniya, C. Das, I. Remy-Speckmann, S. Berendts, A. V. Shevelkov, M. Driess, P. W. Menezes, *Chem. Commun.* **2021**, *57*, 2184.

[93] J. N. Hausmann, S. Mebs, K. Laun, I. Zebger, H. Dau, P. W. Menezes, M. Driess, *Energy Environ. Sci.* **2020**, *13*, 3607.

[94] A Indra, P. W. Menezes, I. Zaharieva, H. Dau, M. Driess, *J. Mater. Chem. A* **2020**, *8*, 2637.

[95] B. Singh, O. Prakash, P. Maiti, P. W. Menezes, A. Indra, *Chem. Commun.* **2020**, *56*, 15036.

[96] C. Walter, P. W. Menezes, M. Driess, *Chem. Sci.* **2021**, *12*, 8603.

[97] X. Liu, J. Meng, J. Zhu, M. Huang, B. Wen, R. Guo, L. Mai, *Adv. Mater.* **2021**, *33*, 2007344.

[98] P. W. Menezes, C. Panda, C. Walter, M. Schwarze, M. Driess, *Adv. Funct. Mater.* **2019**, *29*, 1808632.

[99] W. Zou, C. Sun, K. Zhao, J. Li, X. Pan, D. Ye, Y. Xie, W. Xu, H. Zhao, L. Zhang, *Electrochim. Acta* **2020**, *345*, 136114.

[100] Y. Zhu, H. C. Chen, C. S. Hsu, T. S. Lin, C. J. Chang, S. C. Chang, L. D. Tsai, H. M. Chen, *ACS Energy Lett.* **2019**, *4*, 987.

[101] J. Chen, H. Chen, T. Yu, R. Li, Y. Wang, Z. Shao, S. Song, *EnergyRev.* **2021**, *4*, 566.

[102] L. Gao, X. Cui, C. D. Sewell, J. Li, Z. Lin, *Chem. Soc. Rev.* **2021**, *50*, 8428.

[103] D. Lebedev, R. Ezhov, J. Heras-Domingo, A. Comas-Vives, N. Kaeffer, M. Willinger, X. Solans-Monfort, X. Huang, Y. Pushkar, C. Copéret, *ACS Cent. Sci.* **2020**, *6*, 1189.

[104] H. Y. Yang, Z. L. Chen, P. F. Guo, B. Fei, R. B. Wu, *Appl. Catal., B* **2020**, *261*, 118240.

[105] J. G. Baker, J. R. Schneider, J. A. G. Torres, J. A. Singh, A. J. Mackus, M. Bajdich, S. F. Bent, *ACS Appl. Energy Mater.* **2019**, *2*, 3488.

[106] C. Y. Fu, S. Weng, J. L. Fan, Y. R. Zhang, Y. H. Guo, W. J. Hao, *Chem. Eng. J.* **2022**, *430*, 132881.

[107] T. X. Gentner, R. E. Mulvey, *Angew. Chem., Int. Ed.* **2021**, *60*, 9247.

[108] K. Lu, Y. Liu, F. Lin, I. A. Cordova, S. Gao, B. Li, B. Peng, H. Xu, J. Kaelin, D. Coliz, C. Wang, Y. Shao, Y. Cheng, *J. Am. Chem. Soc.* **2020**, *142*, 12613.

[109] Z. Xiao, W. Zhou, N. Zhang, C. Liao, S. Huang, G. Chen, G. Chen, M. Liu, X. Liu, R. Ma, *Chem. Commun.* **2021**, *57*, 6070.

[110] K. Zhang, R. Zou, *Small* **2021**, *17*, 2100129.

[111] Z. Lu, H. Wang, D. Kong, K. Yan, P. C. Hsu, G. Zheng, H. Yao, Z. Liang, X. Sun, Y. Cui, *Nat. Commun.* **2014**, *5*, 4345.

[112] B. Weng, F. Xu, C. Wang, W. Meng, C. R. Grice, Y. Yan, *Energy Environ. Sci.* **2017**, *10*, 121.

[113] L. Sun, Z. Dai, L. Zhong, Y. Zhao, Y. Cheng, S. Chong, G. Chen, C. Yan, X. Zhang, H. Tan, L. Zhang, K. N. Dinh, S. Li, F. Ma, Q. Yan, *Appl. Catal., B* **2021**, *297*, 120477.

[114] G. Fu, X. Wen, S. Xi, Z. Chen, W. Li, J. Y. Zhang, A. Tadich, R. Wu, D. C. Qi, Y. Du, J. Cheng, K. H. L. Zhang, *Chem. Mater.* **2018**, *31*, 419.

[115] D. Chanda, S. Basu, *Int. J. Hydrogen Energy* **2018**, *43*, 21999.

[116] M. Qu, X. Ding, Z. Shen, M. Cui, F. E. Oropeza, G. Gorni, V. A. de la Peña O'Shea, W. Li, D. C. Qi, K. H. Zhang, *Chem. Mater.* **2021**, *33*, 2062.

[117] A. N. Singh, M. H. Kim, A. Meena, T. U. Wi, H. W. Lee, K. S. Kim, *Small* **2021**, *17*, 2005605.

[118] R. Gond, S. P. Vanam, P. Barpanda, *Chem. Commun.* **2019**, *55*, 11595.

[119] S. Xue, B. Garlyyev, A. Auer, J. Kunze-Liebhäuser, A. S. Bandarenka, *J. Phys. Chem. C* **2020**, *124*, 12442.

[120] Z. Xu, Y. Ying, G. Zhang, K. Li, Y. Liu, N. Fu, X. Guo, F. Yu, H. Huang, *J. Mater. Chem. A* **2020**, *8*, 26130.

2108432 (27 of 31)

[121] S. r. Dresp, F. Dionigi, M. Klingenhof, T. Merzdorf, H. Schmies, J. Drnec, A. Poulain, P. Strasser, *ACS Catal.* **2021**, *11*, 6800.

[122] S. K. Searles, I. Dzidic, P. Kebarle, *J. Am. Chem. Soc.* **1969**, *91*, 2810.

[123] K. Li, D. Xue, *J. Phys. Chem. A* **2006**, *110*, 11332.

[124] Y. Marcus, *Ions in Solution and their Solvation*, John Wiley & Sons, New Jersey **2015**.

[125] X. Li, C. M. Gunathunge, N. Agrawal, H. Montalvo-Castro, J. Jin, M. J. Janik, M. M. Waegele, *J. Electrochem. Soc.* **2020**, *167*, 106505.

[126] A. C. Garcia, T. Touzalin, C. Nieuwland, N. Perini, M. T. Koper, *Angew. Chem., Int. Ed.* **2019**, *58*, 12999.

[127] D. Strmcnik, K. Kodama, D. van der Vliet, J. Greeley, V. R. Stamenkovic, N. Marković, *Nat. Chem.* **2009**, *1*, 466.

[128] H. Wang, J. Wu, A. Dolocan, Y. Li, X. Lü, N. Wu, K. Park, S. Xin, M. Lei, W. Yang, J. B. Goodenough, *Proc. Natl. Acad. Sci. USA* **2019**, *116*, 23473.

[129] J. D. Michael, E. L. Demeter, S. M. Illes, Q. Fan, J. R. Boes, J. R. Kitchin, *J. Phys. Chem. C* **2015**, *119*, 11475.

[130] C. Yang, O. Fontaine, J. M. Tarascon, A. Grimaud, *Angew. Chem., Int. Ed.* **2017**, *56*, 8652.

[131] J. A. D. del Rosario, G. Li, M. F. M. Labata, J. D. Ocon, P. Y. A. Chuang, *Appl. Catal., B-Environ.* **2021**, *288*, 119981.

[132] D. Huang, S. Li, Y. Luo, L. Liao, J. Ye, H. Chen, *Nanoscale* **2019**, *11*, 19429.

[133] J. Zaffran, M. B. Stevens, C. D. Trang, M. Nagli, M. Shehadeh, S. W. Boettcher, M. C. Toroker, *Chem. Mater.* **2017**, *29*, 4761.

[134] M. Görlin, J. H. Stenlid, S. Koroidov, H. Y. Wang, M. Börner, M. Shipilin, A. Kalinko, V. Murzin, O. V. Safonova, M. Nachtegaal, A. Uheida, J. Dutta, M. Bauer, A. Nilsson, O. Diaz-Morales, *Nat. Commun.* **2020**, *11*, 6181.

[135] Y. Wang, Y. Zhao, X. Ding, L. Qiao, *J. Energy Chem.* **2021**, *60*, 451.

[136] V. Dileepkumar, C. Pratapkumar, R. Viswanatha, B. M. Basavaraja, R. R. Maphanga, M. Chennabasappa, N. Srinivasa, S. Ashoka, Z. Chen, S. Rtimi, K. Jayaramulu, R. S. Varma, G. Szekely, M. S. Santosh, *Chem. Eng. J.* **2021**, *426*, 131315.

[137] H. Yu, X. Sun, D. Tang, Y. Huang, W. Zhang, S. Miao, Z. A. Qiao, J. Wang, Z. Zhao, *Int. J. Hydrogen Energy* **2020**, *45*, 6006.

[138] D. A. Henckel, O. M. Lenz, K. M. Krishnan, B. M. Cossairt, *Nano Lett.* **2018**, *18*, 2329.

[139] P. W. Menezes, A. Indra, I. Zaharieva, C. Walter, S. Loos, S. Hoffmann, R. Schlögl, H. Dau, M. Driess, *Energy Environ. Sci.* **2019**, *12*, 988.

[140] P. W. Menezes, C. Walter, B. Chakrabory, J. N. Hausmann, I. Zaharieva, A. Frick, E. Hauff, H. Dau, M. Driess, *Adv. Mater.* **2021**, *33*, 2004098.

[141] J. Kwon, H. Han, S. Jo, S. Choi, K. Y. Chung, G. Ali, K. Park, U. Paik, T. Song, *Adv. Energy Mater.* **2021**, *11*, 2100624.

[142] M. M. Najafpour, T. Ehrenberg, M. Wiechen, P. Kurz, *Angew. Chem., Int. Ed.* **2010**, *49*, 2233.

[143] H. Guo, J. Huang, H. Zhou, F. Zuo, Y. Jiang, K. H. Zhang, X. Fu, Y. Bu, W. Cheng, Y. Sun, *ACS Appl. Mater. Interfaces* **2021**, *13*, 24887.

[144] D. Liu, P. Zhou, H. Bai, H. Ai, X. Du, M. Chen, D. Liu, W. F. Ip, K. H. Lo, C. T. Kwok, S. Chen, S. Wang, C. Xing, X. Wang, H. Pan, *Small* **2021**, *17*, 2101605.

[145] Y. Wu, W. Sun, Z. Zhou, W. Q. Zaman, M. Tariq, L. Cao, J. Yang, *ACS Omega* **2018**, *3*, 2902.

[146] J. O. M. Bockris, T. Otagawa, *J. Electrochem. Soc.* **1984**, *131*, 290.

[147] Y. Zhang, Y. F. Sun, J. L. Luo, *ECS Trans.* **2016**, *75*, 955.

[148] D. He, G. He, H. Jiang, Z. Chen, M. Huang, *Chem. Commun.* **2017**, *53*, 5132.

[149] T. H. Shen, L. Spillane, J. Vavra, T. H. H. Pham, J. Y. Peng, Y. Shao-Horn, V. Tileli, *J. Am. Chem. Soc.* **2020**, *142*, 15876.

[150] R. K. Hona, F. Ramezanipour, *Angew. Chem.* **2019**, *131*, 2082.

[151] R. Sankannavar, A. Sarkar, *Int. J. Hydrogen Energy* **2018**, *43*, 4682.

[152] G. Chen, W. Zhou, D. Guan, J. Sunarso, Y. Zhu, X. Hu, W. Zhang, Z. Shao, *Sci. Adv.* **2017**, *3*, 1603206.

[153] E. Fabbri, M. Nachtegaal, T. Binninger, X. Cheng, B.-J. Kim, J. Durst, F. Bozza, T. Graule, R. Schäublin, L. Wiles, M. Pertoso, N. Danilovic, K. E. Ayers, T. J. Schmidt, *Nat. Mater.* **2017**, *16*, 925.

[154] J. W. Zhao, Z. X. Shi, C. F. Li, Q. Ren, G. R. Li, *ACS Mater. Lett.* **2021**, *3*, 721.

[155] F. Dong, L. Li, Z. Kong, X. Xu, Y. Zhang, Z. Gao, B. Dongyang, M. Ni, Q. Liu, Z. Lin, *Small* **2021**, *17*, 2006638.

[156] H. Chen, L. Shi, X. Liang, L. Wang, T. Asefa, X. Zou, *Angew. Chem., Int. Ed.* **2020**, *59*, 19654.

[157] J. Miao, Z. Lang, X. Zhang, W. Kong, O. Peng, Y. Yang, S. Wang, J. Cheng, T. He, A. Amini, Q. Wu, Z. Zheng, Z. Tang, C. Cheng, *Adv. Funct. Mater.* **2019**, *29*, 1805893.

[158] C. W. Song, J. Lim, H. B. Bae, S.-Y. Chung, *Energy Environ. Sci.* **2020**, *13*, 4178.

[159] S. R. Ede, C. N. Collins, C. D. Posada, G. George, H. Wu, W. D. Ratcliff, Y. Lin, J. Wen, S. Han, Z. Luo, *ACS Catal.* **2021**, *11*, 4327.

[160] E. Tsuji, T. Motohashi, H. Noda, D. Kowalski, Y. Aoki, H. Tanida, J. Niikura, Y. Koyama, M. Mori, H. Arai, T. Ioroi, N. Fujiwara, Y. Uchimoto, Z. Ogumi, H. Habazaki, *ChemSusChem* **2017**, *10*, 2864.

[161] J. Kim, X. Yin, K. C. Tsao, S. Fang, H. Yang, *J. Am. Chem. Soc.* **2014**, *136*, 14646.

[162] D. Kowalski, H. Kiuchi, T. Motohashi, Y. Aoki, H. Habazaki, *ACS Appl. Mater. Interfaces* **2019**, *11*, 28823.

[163] B. J. Kim, X. Cheng, D. F. Abbott, E. Fabbri, F. Bozza, T. Graule, I. E. Castelli, L. Wiles, N. Danilovic, K. E. Ayers, N. Marzari, T. J. Schmidt, *Adv. Funct. Mater.* **2018**, *28*, 1804355.

[164] C. K. Chua, Z. Sofer, O. Jankovský, M. Pumera, *ChemPhysChem* **2015**, *16*, 769.

[165] C. Ramana, M. Bandi, A. N Nair, F. S. Manciu, S. Sreenivasan, V. Shutthanandan, *ACS Appl. Energy Mater.* **2021**, *4*, 1313.

[166] M. Bozorgchenani, P. Fischer, J. Schnaidt, T. Diemant, R. M. Schwarz, M. Marinaro, M. Wachtler, L. Jörissen, R. J. Behm, *ChemElectroChem* **2018**, *5*, 2600.

[167] T. Okada, H. Abe, A. Murakami, T. Shimizu, K. Fujii, T. Wakabayashi, M. Nakayama, *Langmuir* **2020**, *36*, 5227.

[168] M. Kunitski, N. Eicke, P. Huber, J. Köhler, S. Zeller, J. Voigtsberger, N. Schlott, K. Henrichs, H. Sann, F. Trinter, L. Ph H Schmidt, A. Kalinin, M. S Schöffler, T. Jahnke, M. Lein, R. Dörner, *Nat. Commun.* **2019**, *10*, 1.

[169] F. H. Zhang, L. Yu, L. B. Wu, D. Luo, Z. F. Ren, *Trends Chem.* **2021**, *3*, 485.

[170] L. B. Wu, L. Yu, F. H. Zhang, B. McElhenny, D. Luo, A. Karim, S. Chen, Z. F. Ren, *Adv. Funct. Mater.* **2021**, *31*, 2006484.

[171] Z. Zeng, X. Xu, Z. Zhang, Z. Gao, M. Luo, Z. Yin, C. Zhang, J. Xu, B. Huang, F. Luo, Y. Du, C. Yan, *Chem. Soc. Rev.* **2020**, *49*, 1109.

[172] Y. Zhu, W. Zhou, Z. Shao, *Small* **2017**, *13*, 1603793.

[173] C. Sun, J. A. Alonso, J. Bian, *Adv. Energy Mater.* **2021**, *11*, 2000459.

[174] B. Han, K. A. Stoerzinger, V. Tileli, A. D. Gamalski, E. A. Stach, Y. Shao-Horn, *Nat. Mater.* **2017**, *16*, 121.

[175] J. Hwang, R. R. Rao, L. Giordano, Y. Katayama, Y. Yu, Y. Shao-Horn, *Science* **2017**, *358*, 751.

[176] B. J. Kim, D. F. Abbott, X. Cheng, E. Fabbri, M. Nachtegaal, F. Bozza, I. E. Castelli, D. Lebedev, R. Schäublin, C. Coperet, T. Graule, N. Marzari, T. J. Schmidt, *ACS Catal.* **2017**, *7*, 3245.

[177] L. Wang, K. A. Stoerzinger, L. Chang, J. Zhao, Y. Li, C. S. Tang, X. Yin, M. E. Bowden, Z. Yang, H. Guo, L. You, R. Guo, J. Wang, K. Ibrahim, J. Chen, A. Rusydi, J. Wang, S. A. Chambers, Y. Du, *Adv. Funct. Mater.* **2018**, *28*, 1803712.

[178] H. Xu, B. Wang, C. Shan, P. Xi, W. Liu, Y. Tang, *ACS Appl. Mater. Interfaces* **2018**, *10*, 6336.

2108432 (28 of 31)

**ADVANCED
SCIENCE NEWS**

www.advancedsciencenews.com

**ADVANCED
MATERIALS**

www.advmat.de

[179] D. A. Kuznetsov, M. A. Naeem, P. V. Kumar, P. M. Abdala, A. Fedorov, C. R. Müller, *J. Am. Chem. Soc.* **2020**, *142*, 7883.

[180] J. Kim, P. C. Shih, K. C. Tsao, Y. T. Pan, X. Yin, C. J. Sun, H. Yang, *J. Am. Chem. Soc.* **2017**, *139*, 12076.

[181] Y. N. Zhou, R. Y. Fan, S. Y. Dou, B. Dong, Y. Ma, W. L. Yu, M. X. Li, Y. L. Zhou, C. G. Liu, Y. M. Chai, *J. Energy Chem.* **2021**, *59*, 299.

[182] J. Kim, P. C. Shih, Y. Qin, Z. Al-Bardan, C. J. Sun, H. Yang, *Angew. Chem., Int. Ed.* **2018**, *57*, 13877.

[183] W. Gao, F. Ma, C. Wang, D. Wen, *J. Power Sources* **2020**, *450*, 227654.

[184] W. Gao, M. Yan, H. Y. Cheung, Z. Xia, X. Zhou, Y. Qin, C. Y. Wong, J. C. Ho, C. R. Chang, Y. Qu, *Nano Energy* **2017**, *38*, 290.

[185] T. X. Nguyen, Y. C. Liao, C. C. Lin, Y. H. Su, J. M. Ting, *Adv. Funct. Mater.* **2021**, *31*, 2101632.

[186] F. Cheng, Z. Li, L. Wang, B. Yang, J. Lu, L. Lei, T. Ma, Y. Hou, *Mater. Horiz.* **2021**, *8*, 556.

[187] M. Jakšić, *Int. J. Hydrogen Energy* **1987**, *12*, 727.

[188] M. H. Miles, *J. Electroanal. Chem. Interfacial Electrochem.* **1975**, *60*, 89.

[189] H. Tamura, C. Iwakura, T. Kitamura, *J. Less-Common Met.* **1983**, *89*, 567.

[190] T. Kitamura, C. Iwakura, H. Tamura, *Chem. Lett.* **1981**, *10*, 965.

[191] D. Cardoso, L. Amaral, D. Santos, B. Šljukić, C. Sequeira, D. Macciò, A. Saccone, *Int. J. Hydrogen Energy* **2015**, *40*, 4295.

[192] F. Rosalbino, S. Delsante, G. Borzone, E. Angelini, *J. Alloys Compd.* **2007**, *429*, 270.

[193] M. A. Dominguez-Crespo, A. M. Torres-Huerta, B. Brachetti-Sibaja, A. Flores-Vela, *Int. J. Hydrogen Energy* **2011**, *36*, 135.

[194] F. Rosalbino, D. Macciò, E. Angelini, A. Saccone, S. Delfino, *Int. J. Hydrogen Energy* **2008**, *33*, 2660.

[195] J. Huang, H. Sheng, R. D. Ross, J. Han, X. Wang, B. Song, S. Jin, *Nat. Commun.* **2021**, *12*, 3036.

[196] P. L. Kharel, P. M. Cuillier, K. Fernando, F. P. Zamborini, B. W. Alphenaar, *J. Phys. Chem. C* **2018**, *122*, 15090.

[197] W. Gao, D. Wen, J. Ho, Y. Qu, *Mater. Today Chem.* **2019**, *12*, 266.

[198] Y. Liu, C. Ma, Q. Zhang, W. Wang, P. Pan, L. Gu, D. Xu, J. Bao, Z. Dai, *Adv. Mater.* **2019**, *31*, 1900062.

[199] H. Sun, C. Tian, G. Fan, J. Qi, Z. Liu, Z. Yan, F. Cheng, J. Chen, C. P. Li, M. Du, *Adv. Funct. Mater.* **2020**, *30*, 1910596.

[200] J. Xia, H. Zhao, B. Huang, L. Xu, M. Luo, J. Wang, F. Luo, Y. Du, C. H. Yan, *Adv. Funct. Mater.* **2020**, *30*, 1908367.

[201] H. Xu, J. Cao, C. Shan, B. Wang, P. Xi, W. Liu, Y. Tang, *Angew. Chem., Int. Ed.* **2018**, *57*, 8654.

[202] K. Obata, K. Takanabe, *Angew. Chem., Int. Ed.* **2018**, *57*, 1616.

[203] L. Nie, D. Mei, H. Xiong, B. Peng, Z. Ren, X. I. P. Hernandez, A. DeLaRiva, M. Wang, M. H. Engelhard, L. Kovarik, A. K. Datye, Y. Wang, *Science* **2017**, *358*, 1419.

[204] Y. Tang, Y. Wei, Z. Wang, S. Zhang, Y. Li, L. Nguyen, Y. Li, Y. Zhou, W. Shen, F. F. Tao, P. Hu, *J. Am. Chem. Soc.* **2019**, *141*, 7283.

[205] X. Gao, G. Yu, L. Zheng, C. Zhang, H. Li, T. Wang, P. An, M. Liu, X. Qiu, W. Chen, *ACS Appl. Energy Mater.* **2019**, *2*, 966.

[206] P. W. Menezes, C. Panda, S. Garai, C. Walter, A. Guiet, M. Driess, *Angew. Chem.* **2018**, *130*, 15457.

[207] B. Chakraborty, R. Beltrán-Suito, J. N. Hausmann, S. Garai, M. Driess, P. W. Menezes, *Adv. Energy Mater.* **2020**, *10*, 2001377.

[208] A. Subramanian, M. A. Mahadik, J. W. Park, I. K. Jeong, H. S. Chung, H. H. Lee, S. H. Choi, W. S. Chae, J. S. Jang, *Electrochim. Acta* **2019**, *319*, 444.

[209] M. Yu, G. Li, C. Fu, E. Liu, K. Manna, E. Budiyanto, Q. Yang, C. Felser, H. Tüysüz, *Angew. Chem., Int. Ed.* **2021**, *60*, 5800.

[210] W. He, F. Wang, D. Jia, Y. Li, L. Liang, J. Zhang, Q. Hao, C. Liu, H. Liu, J. Zhao, *Nanoscale* **2020**, *12*, 24244.

[211] J. N. Hausmann, E. M. Heppke, R. Beltrán-Suito, J. Schmidt, M. Mühlbauer, M. Lerch, P. W. Menezes, M. Driess, *ChemCatChem* **2020**, *12*, 1161.

[212] G. D'Olimpio, S. Nappini, M. Vorokhta, L. Lozzi, F. Genuzio, T. O. Menteş, V. Paolucci, B. Gürbulak, S. Duman, L. Ottaviano, A. Locatelli, F. Bondino, D. W. Boukhvalov, A. Politano, *Adv. Funct. Mater.* **2020**, *30*, 2005466.

[213] C. Wang, H. Shang, Y. Wang, J. Li, S. Guo, J. Guo, Y. Du, *Nanoscale* **2021**, *13*, 7279.

[214] S. F. Zai, Y. T. Zhou, C. C. Yang, Q. Jiang, *Chem. Eng. J.* **2021**, *421*, 127856.

[215] T. A. Shifa, K. Yusupov, G. Solomon, A. Gradone, R. Mazzaro, E. Cattaruzza, A. Vomiero, *ACS Catal.* **2021**, *11*, 4520.

[216] S. F. Zai, A. Q. Dong, J. Li, Z. Wen, C. C. Yang, Q. Jiang, *J. Mater. Chem. A* **2021**, *9*, 6223.

[217] E. P. Alsaç, A. Whittingham, Y. Liu, R. D. L. Smith, *Chem. Mater.* **2019**, *31*, 7522.

[218] G. Shao, X. X. Xue, B. Wu, Y. C. Lin, M. Ouzounian, T. S. Hu, Y. Xu, X. Liu, S. Li, K. Suenaga, Y. Feng, S. Liu, *Adv. Funct. Mater.* **2020**, *30*, 1906069.

[219] S. Sarkar, A. Rawat, T. Das, M. Gaboardi, S. Chakraborty, C. P. Vinod, S. C. Peter, *ChemSusChem* **2021**, *14*, 3074.

[220] H. Zhang, W. Cheng, D. Luan, X. W. Lou, *Angew. Chem., Int. Ed.* **2021**, *60*, 13177.

[221] W. H. Lai, H. Wang, L. Zheng, Q. Jiang, Z. C. Yan, L. Wang, H. Yoshikawa, D. Matsumura, Q. Sun, Y. X. Wang, Q. Gu, J. Z. Wang, H. K. Liu, S. L. Chou, S. X. Dou, *Angew. Chem., Int. Ed.* **2020**, *59*, 22171.

[222] B. Gao, Y. Zhao, X. Du, Y. Chen, B. Guan, Y. Li, Y. Li, S. Ding, H. Zhao, C. Xiao, Z. Song, *J. Mater. Chem. A* **2021**, *9*, 8394.

[223] M. Wang, W. Zhang, F. Zhang, Z. Zhang, B. Tang, J. Li, X. Wang, *ACS Catal.* **2019**, *9*, 1489.

[224] Z. Ji, J. Liu, Y. Deng, S. Zhang, Z. Zhang, P. Du, Y. Zhao, X. Lu, *J. Mater. Chem. A* **2020**, *8*, 14680.

[225] J. Jian, L. Yuan, H. Qi, X. Sun, L. Zhang, H. Li, H. Yuan, S. Feng, *ACS Appl. Mater. Interfaces* **2018**, *10*, 40568.

[226] H. S. Stein, D. Guevarra, A. Shinde, R. J. Jones, J. M. Gregoire, J. A. Haber, *Mater. Horiz.* **2019**, *6*, 1251.

[227] S. Li, Z. Li, R. Ma, C. Gao, L. Liu, L. Hu, J. Zhu, T. Sun, Y. Tang, D. Liu, J. Wang, *Angew. Chem., Int. Ed.* **2021**, *60*, 3773.

[228] J. Masa, S. Piontek, P. Wilde, H. Antoni, T. Eckhard, Y. T. Chen, M. Muhler, U. P. Apfel, W. Schuhmann, *Adv. Energy Mater.* **2019**, *9*, 1900796.

[229] S. Ju, J. Feng, P. Zou, W. Xu, S. Wang, W. Gao, H. J. Qiu, J. Huo, J. Q. Wang, *J. Mater. Chem. A* **2020**, *8*, 3246.

[230] D. Liu, X. Fan, X. Wang, D. Hu, C. Xue, Y. Liu, Y. Wang, X. Zhu, J. Guo, H. Lin, Y. Li, J. Zhong, D. Li, X. Bu, P. Feng, T. Wu, *Chem. Mater.* **2018**, *31*, 553.

[231] Z. Du, J. Qian, J. Bai, H. Li, M. Wang, X. Zhao, D. Xiong, *Inorg. Chem.* **2020**, *59*, 9889.

[232] J. Yin, J. Jin, H. Lin, Z. Yin, J. Li, M. Lu, L. Guo, P. Xi, Y. Tang, C. H. Yan, *Adv. Sci.* **2020**, *7*, 1903070.

[233] Y. Zhao, S. Wei, K. Pan, Z. Dong, B. Zhang, H. H. Wu, Q. Zhang, J. Lin, H. Pang, *Chem. Eng. J.* **2021**, *421*, 129645.

[234] R. Beltrán-Suito, V. Forstner, J. N. Hausmann, S. Mebs, J. Schmidt, I. Zaharieva, K. Laun, I. Zebger, H. Dau, P. W. Menezes, M. Driess, *Chem. Sci.* **2020**, *11*, 11834.

[235] A. Grimaud, O. Diaz-Morales, B. Han, W. T. Hong, Y. L. Lee, L. Giordano, K. A. Stoerzinger, M. T. M. Koper, Y. Shao-Horn, *Nat. Chem.* **2017**, *9*, 457.

[236] J. N. Hausmann, R. Beltrán-Suito, S. Mebs, V. Hlukhyy, T. F. Fässler, H. Dau, M. Driess, P. W. Menezes, *Adv. Mater.* **2021**, *33*, 2008823.

[237] P. W. Menezes, S. Yao, R. Beltrán-Suito, J. N. Hausmann, P. V. Menezes, M. Driess, *Angew. Chem., Int. Ed.* **2021**, *60*, 4640.

[238] Y. L. Pan, X. M. Xu, Y. J. Zhong, L. Ge, Y. B. Chen, J. M. Veder, D. Q. Guan, R. O'Hayre, M. R. Li, G. X. Wang, H. Wang, W. Zhou, Z. P. Shao, *Nat. Commun.* **2020**, *11*, 2002.

[239] B. Yang, N. Zhang, G. Chen, K. Liu, J. Yang, A. Pan, M. Liu, X. Liu, R. Ma, T. Qiu, *Appl. Catal., B-Environ.* **2020**, *260*, 118184.

[240] S. Ogawa, Y. Ogino, M. Yonemura, T. Fukunaga, H. Kiuchi, K. Nakayama, R. Ishikawa, Y. Ikuhara, Y. Doi, K. Suzuki, M. Saito, T. Motohashi, *Chem. Mater.* **2020**, *32*, 6847.

[241] D. Böhm, M. Beetz, M. Schuster, K. Peters, A. G. Hufnagel, M. Döblinger, B. Böller, T. Bein, D. Fattakhova-Rohlfing, *Adv. Funct. Mater.* **2020**, *30*, 1906670.

[242] H. Chen, X. Ai, W. Liu, Z. Xie, W. Feng, W. Chen, X. Zou, *Angew. Chem.* **2019**, *131*, 11531.

[243] J. Suntivich, K. J. May, H. A. Gasteiger, J. B. Goodenough, Y. Shao-Horn, *Science* **2011**, *334*, 1383.

[244] J. T. Mefford, X. Rong, A. M. Abakumov, W. G. Hardin, S. Dai, A. M. Kolpak, K. P. Johnston, K. J. Stevenson, *Nat. Commun.* **2016**, *7*, 11053.

[245] J. S. Yoo, Y. Liu, X. Rong, A. M. Kolpak, *J. Phys. Chem. Lett.* **2018**, *9*, 1473.

[246] J. S. Yoo, X. Rong, Y. Liu, A. M. Kolpak, *ACS Catal.* **2018**, *8*, 4628.

[247] X. Rong, J. Parolin, A. M. Kolpak, *ACS Catal.* **2016**, *6*, 1153.

[248] Y. Wu, Y. Zhang, Y. Wang, Z. He, Z. Gu, S. You, *Int. J. Hydrogen Energy* **2021**, *46*, 26930.

[249] D. B. Hibbert, C. R. Churchill, *J. Chem. Soc., Faraday Trans. 1* **1984**, *80*, 1965.

[250] Z. F. Huang, J. Song, Y. Du, S. Xi, S. Dou, J. Nsanzimana, C. Wang, Z. J. Xu, X. Wang, *Nat. Energy* **2019**, *4*, 329.

[251] Y. Surendranath, M. W. Kanan, D. G. Nocera, *J. Am. Chem. Soc.* **2010**, *132*, 16501.

[252] H. Yuan, S. Wang, Z. Ma, M. Kundu, B. Tang, J. Li, X. Wang, *Chem. Eng. J.* **2021**, *404*, 126474.

[253] L. Wu, L. Yu, Q. Zhu, B. Mcelhenny, F. Zhang, C. Wu, X. Xing, J. Bao, S. Chen, Z. Ren, *Nano Energy* **2021**, *83*, 105838.

[254] C. Zhang, G. Yu, R. Ku, X. Huang, W. Chen, *Appl. Surf. Sci.* **2019**, *481*, 272.

[255] A. Maiti, S. K. Srivastava, *ACS Appl. Mater. Interfaces* **2020**, *12*, 7057.

[256] K. Ham, S. Hong, S. Kang, K. Cho, J. Lee, *ACS Energy Lett.* **2021**, *6*, 364.

[257] H. Liu, X. H. Zhang, Y. X. Li, X. Li, C. K. Dong, D. Y. Wu, C. C. Tang, S. L. Chou, F. Fang, X. W. Du, *Adv. Energy Mater.* **2020**, *10*, 1902521.

[258] S. Tang, X. Zhou, T. Liu, S. Zhang, T. Yang, Y. Luo, E. Sharman, J. Jiang, *J. Mater. Chem. A* **2019**, *7*, 26261.

[259] Z. Cui, R. Sa, W. Du, X. Chiao, Q. Li, Z. Ma, *Appl. Surf. Sci.* **2021**, *542*, 148535.

[260] W. Hao, R. Wu, H. Yang, Y. Guo, *J. Mater. Chem. A* **2019**, *7*, 12440.

[261] R. Zhang, X. Ren, S. Hao, R. X. Ge, Z. Liu, A. M. Asiri, L. Chen, Q. J. Zhang, X. P. Sun, *J. Mater. Chem. A* **2018**, *6*, 1985.

[262] J. X. Feng, S. H. Ye, H. Xu, Y. X. Tong, G. R. Li, *Adv. Mater.* **2016**, *28*, 4698.

[263] C. G. Kuai, Z. R. Xu, C. Xi, A. Y. Hu, Z. J. Yang, Y. Zhang, C. J. Sun, L. X. Li, D. Sokaras, C. K. Dong, S. Z. Qiao, X. W. Du, F. Lin, *Nat. Catal.* **2020**, *3*, 743.

[264] C. G. Kuai, C. Xi, A. Y. Hu, Y. Zhang, Z. R. Xu, D. Nordlund, C. J. Sun, C. A. Cadigan, R. M. Richards, L. X. Li, C. K. Dong, X. W. Du, F. Lin, *J. Am. Chem. Soc.* **2021**, *143*, 18519.

[265] C. Feng, F. Z. Wang, Z. Liu, M. Nakabayashi, Y. Q. Xiao, Q. G. Zeng, J. Fu, Q. B. Wu, C. H. Cui, Y. F. Han, N. Shibata, K. Domen, I. D. Sharp, Y. B. Li, *Nat. Commun.* **2021**, *12*, 5980.

[266] W. T. Thompson, M. H. Kaye, C. W. Bale, A. D. Pelton, in *Uhlig's Corrosion Handbook, Pourbaix Diagrams for Multielement Systems*, 3rd ed., Wiley, New York **2011**, p. 103.

[267] S. Dutta, H. Han, M. Je, H. Choi, J. Kwon, K. Park, A. Indra, K. M. Kim, U. Paik, T. Song, *Nano Energy* **2020**, *67*, 104245.

[268] D. Channei, S. Phanichphant, A. Nakaruk, S. Mofarah, P. Koshy, C. Sorrell, *Catalysts* **2017**, *7*, 45.

[269] O. Pensado-Rodriguez, M. Urquidi-Macdonald, D. D. Macdonald, *J. Electrochem. Soc.* **1999**, *146*, 1318

[270] N. Artrith, W. Sailuam, S. Limpijumnong, A. M. Kolpak, *Phys. Chem. Chem. Phys.* **2016**, *18*, 29561.

[271] S. K. Yadav, A. L. Ramanathan, M. Kumar, S. Chidambaram, Y. P. Gautam, C. Tiwari, *Environ. Earth Sci.* **2020**, *79*, 154.

[272] C. Z. Yuan, K. S. Hui, H. Yin, S. Q. Zhu, J. T. Zhang, X. L. Wu, X. T. Hong, W. Zhou, X. Fan, F. Bin, F. M. Chen, K. N. Hui, *ACS Mater. Lett.* **2021**, *3*, 752.

[273] X. C. Du, J. W. Huang, J. J. Zhang, Y. C. Yan, C. Y. Wu, Y. Hu, C. Y. Yan, T. Y. Lei, W. Chen, C. Fan, J. Xiong, *Angew. Chem., Int. Ed.* **2019**, *58*, 4484.

[274] H. Wang, Z. Lu, S. Xu, D. Kong, J. J. Cha, G. Zheng, P. C. Hsu, K. Yan, D. Bradshaw, F. B. Prinz, Y. Cui, *Proc. Natl. Acad. Sci. USA* **2013**, *110*, 19701.

[275] R. Khan, M. T. Mehran, S. R. Naqvi, A. H. Khoja, K. Mahmood, F. Shahzad, S. Hussain, *Int. J. Energy Res.* **2020**, *44*, 9714.

[276] X. Y. Yu, X. W. Lou, *Adv. Energy Mater.* **2018**, *8*, 1701592.

[277] H. Han, K. M. Kim, J. H. Ryu, H. J. Lee, J. Woo, G. Ali, K. Y. Chung, T. Kim, S. Kang, S. Choi, J. Kwon, Y. C. Chung, S. W. Mhin, T. Song, *Nano Energy* **2020**, *75*, 104945.

Ziliang Chen received his Ph. D. in Materials Science from Fudan University, China in 2018. After that, he worked as a postdoctoral researcher at Fudan University and the University of Maryland. Now he is an associate professor in Soochow University and an AvH research fellow in Prof. Driess' and Dr. Menezes' group in Technische Universität Berlin. His current research interests focus on the synthesis of novel metal-mediated functional materials and their applications in energy conversion and storage, such as water splitting, secondary batteries, and hydrogen storage.

Hongyuan Yang is currently pursuing his Ph.D. degree under the supervision of Dr. P. W. Menezes and Prof. M. Driess at the Department of Metalorganics and Inorganic Materials, Technical University of Berlin. He attained his master's degree in Materials Physicals and Chemistry from Fudan University, China in 2020. In 2017, he received his bachelor's degree in Inorganic Non-metallic Materials Engineering from Changzhou University, China. His current research interests focus on photo/electrocatalysis, especially for water splitting.

Zhenhui Kang is currently a professor in the Institute of Functional Nano and Soft Materials Laboratory (FUNSOM), Jiangsu Key Laboratory for Carbon-Based Functional Materials & Devices, Soochow University, P. R. China. He received his Ph.D. in Chemistry from Northeast Normal University, China in 2005. He is a recipient of the National Science Fund award for Distinguished Young Scholars. His main research interests are in the fields of quantum-inspired synthesis, self-assembly of functional materials, and hybridization of carbon with metal materials, as well as their application in catalysis, energy conversion, nanodevices, and bioapplication.

Matthias Driess is a full professor of metalorganics and inorganic materials at the Department of Chemistry of Technische Universität Berlin. He obtained his Ph.D. degree and completed his habilitation at the University of Heidelberg in Germany. He serves as a deputy of the Cluster of Excellence UniSysCat and is a Director of the UniSysCat-BASF SE joint lab BasCat, and of the Chemical Invention Factory (CIF) for Start-ups in Green Chemistry. He is a member of the German National Academy of Sciences (Leopoldina), the Berlin-Brandenburg Academy of Sciences and Humanities, and the European Academy of Sciences.

Prashanth W. Menezes is a head of materials chemistry for thin film catalysis group at CatLab of Helmholtz-Zentrum Berlin für Materialien und Energie and inorganic materials group at Technische Universität Berlin. He received his Ph.D. from Max Planck Institute for Chemical Physics of Solids in Dresden, following which he moved to Technische Universität München and then to Technische Universität Berlin to work on energy catalysis. His research focuses on the design, development, and structural understanding of novel unconventional catalysts in hetero-geneous catalysis, especially in the area of redox oxygen catalysis, (photo)electrocatalytic water splitting as well as electrochemical redox reactions.